Rúben Rodrigues Ferreira

Licenciado em Química Aplicada

Flavylium-Functionalized Carbon Quantum Dots

Dissertação para obtenção do Grau de Mestre em
Química Bioorgânica

Orientador: Jorge Parola, Professor Associado, LAQV-REQUIMTE-FCT/UNL

Co-orientador: César Laia, Investigador Auxiliar, LAQV-REQUIMTE-FCT/UNL

Júri:

Presidente: Professora Doutora Paula Cristina de Sério Branco

Arguentes: Professor Doutor José Ricardo Ramos Franco Tavares

Vogais: Professor Doutor António Jorge Dias Parola

FACULDADE DE CIÊNCIAS E TECNOLOGIA
UNIVERSIDADE NOVA DE LISBOA

Outubro, 2016

Flavylium-Functionalized Carbon Quantum Dots

“The real friendship is like fluorescence,

it shines better when everything has darken.”

Agradecimentos

Gostaria de começar por agradecer aos meus orientadores, César Laia e Jorge Parola, pela orientação dada durante o decorrer desta tese de mestrado, bem como durante o meu projeto de licenciatura e projetos de Química Física. Já são 4 anos a aturar-me, a acreditar em mim e a ensinar-me.

Queria também agradecer ao grupo de fotoquímica, pela amabilidade com que me receberam e o apoio que me deram sempre que precisei.

Aos meus pais, pelo suporte financeiro que me permitiu ter esta formação académica.

Aos meus amigos/colegas que estiveram comigo nos bons e maus momentos, com os quais tive a oportunidade de trocar conhecimentos e crescer como pessoa.

Por último, gostaria de agradecer à FCT-UNL, que tem sido a minha segunda casa durante estes últimos 5 anos.

Abstract

The goal of this master thesis was the functionalization of carbon quantum dots (CQDs) with flavylium salts. CQDs were synthesized through the hydrothermal method using citric acid as a carbon precursor and ethylenediamine as a basic catalyst and passivation agent. Since these CQDs are known to bear primary amines groups at their surface, flavylium derivatives with tails containing carboxyl groups were synthesized, 7-hydroxy-4'-methylcarboxyflavylium and 7-hydroxy-4'-methylcarboxy-4-phenylflavylium, in order to functionalize the CQDs with these kind of molecules, using EDC as coupling agent.

CQDs were successfully functionalized with these two flavylium, however, the focus of this thesis was the study of CQDs functionalized with 7-hydroxy-4'-methylcarboxy-4-phenylflavylium, due to its simplest equilibrium between $\mathbf{AH^+}$ and **A**. CQDs were characterized by UV-Vis and steady-state fluorescence spectroscopy.

Keywords: Carbon quantum dots; Flavylium; EDC; Functionalization

Resumo

O objetivo desta tese de mestrado foi a funcionalização de *quantum dots* de carbono (CQDs) com sais de flavílio. Os CQDs foram sintetizados através do método hidrotérmico usando ácido cítrico como precursor de carbono e etilenodiamina como catalisador e agente de emcapsulamento. Uma vez que os CQDs possuem aminas primárias na sua superfície, foram sintetizados derivados de flavílio com caudas contendo grupos carboxilo, 7-hidroxi-4'-metilcarboxiflavilio e 7-hidroxi-4'-metilcarboxi-4-phenilflavilio, a fim de funcionalizar os CQDs com este tipo de moléculas, usando EDC como agente de acoplamento.

Os CQDs foram funcionalizados com êxito com estes dois flavílios, no entanto, o foco desta tese foi o estudo de CQDs funcionalizados com o 7-hidroxi-4'-metilcarboxi-4-phenilflavilio, uma vez que possuí um equilíbrio mais simples, entre $\mathbf{AH^+}$ e **A**. Os CQDs funcionalizados foram caracterizados por espectroscopia de UV-Vis e fluorescência no estado estacionário.

Palavras-chave: Quantum dots de carbono; Flavílios; EDC; Funcionalização

List of abbreviations and symbols

δ	Chemical shift
ε	Molar absorptivity
φ	Quantum yield
A^-	Ionized quinoidal base
AH^+	Flavylium cation
AIBN	Azobisisobutyronitrile
ANS	1-Anilinonaphthalene-8-Sulfonic Acid
B	Hemiacetal
Bt	Benzotriazole
Cc	*Cis*-chalcone
CD	Carbon dot
CEE	Crosslink enhanced emission
CND	Carbon nanodot
CNP	Carbon nanoparticle
CQD	Carbon quantum dot
Ct	*Trans*-chalcone
Ct^-	Ionized *Trans*-chalcone

DCC	N,N'-Dicyclohexylcarbodiimide
EA	Elemental analysis
EDA	Ethylenediamine
EDC	1-Ethyl-3-(3-dimethylaminopropyl)carbodiimide
EDTA	Ethylenediaminetetraacetic acid
ESI/MS	Electrospray Ionisation / Mass Spectrometry
ESPT	Excited state proton transfer
GQD	Graphene quantum dot
HOMO	Highest occupied molecular orbital
HR-TEM	High-resolution transmission electron microscopy
LUMO	Lowest unoccupied molecular orbital
MWCO	Molecular weight cut-off
NBS	N-Bromosuccinimide
NHS	N-Hydroxysuccinimide
NMR	Nuclear magnetic resonance
PD	Polymer dot
PL	Photoluminescence
QD	Quantum dot
QY	Quantum yield
SPC	Single Photon Counting
Sw-CNT	Single-walled carbon nanotube
TEM	Transmission electron microscopy
THF	Tetrahydrofuran

Table of Contents

Figures Index

Schemes Index

Tables Index

1

Introduction

1.1. Semiconductors

In semiconductors, light absorption generally leads to an electron being excited from the valence to the conduction band, leaving behind a hole. The electron and the hole can still be attracted to each other by electrostatic Coulomb forces, forming an exciton (the electron-hole pair). When this exciton recombines i.e. the electron resumes its ground state, the exciton's energy can be emitted as light. This phenomenon is commonly known as photoluminescence (PL).[1]

In a simplified model, the energy of the emitted photon can be understood as the sum of the band gap energy between the highest occupied level and the lowest unoccupied energy level, the confinement energies of the hole and the excited electron, and the bound energy of the exciton.

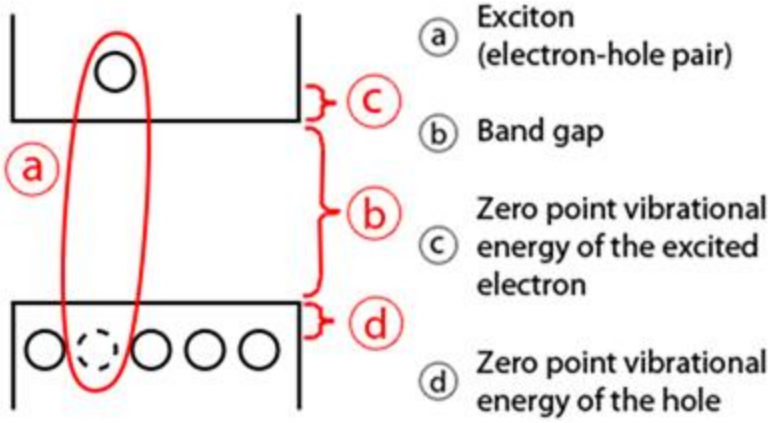

Figure 1 – Schematic representation of an exciton and the corresponding energy levels

1.2. Quantum dots

Quantum dots (QDs) are semiconductor spherical nanoparticles, with a size typically under 10 nm.[2,3] These nanoparticles exhibit optical and electronic properties different from those observed in bulk particles. One property with special interest is their size-dependent fluorescence. This is due to a phenomena known as "quantum confinement".[4, 5]

Quantum confinement results from electrons and electron holes being squeezed into a dimension that approaches a critical quantum measurement, called the exciton Bohr radius, this represents the distance between the electron and the hole. As the confining dimension decreases and reaches a certain limit, the energy spectrum becomes discrete. This means that instead of having a continuous energy band, composed of various energy states closely staked together, QDs have discrete energy states. This discretization results in electronic transitions that vary by QD size. Larger QD have closer electronic states than smaller quantum dots which means that the energy required to excite an electron from HOMO to the LUMO is lower than the same electronic transition in a smaller QD. This quantum confinement effect can be observed as a red shift in absorbance spectra for nanocrystals with larger diameters.

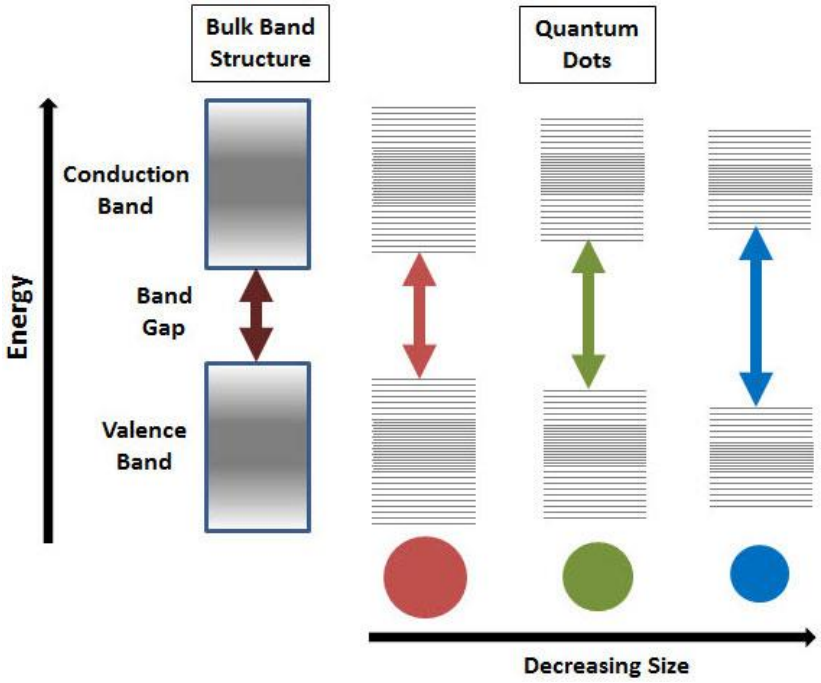

Figure 2 – Splitting of energy levels in quantum dots due to the quantum confinement effect

As a consequence, larger QDs (radius of 5 – 6 nm) emit at longer wavelengths resulting in emission colours such as orange or red. Smaller QDs (radius of 2 – 3 nm) emit shorter wavelengths resulting in colours like blue and green, although the specific colours and sizes vary depending on the exact composition of the QD.

A spherical nanoparticle can have quantum confinement in three dimensions, but is also possible to have quantum confinement in only two dimensions (quantum wire) and in one dimension (quantum well). This indicates that the nanoparticles shape may also play an important role in the optical and electronic proprieties.[6]

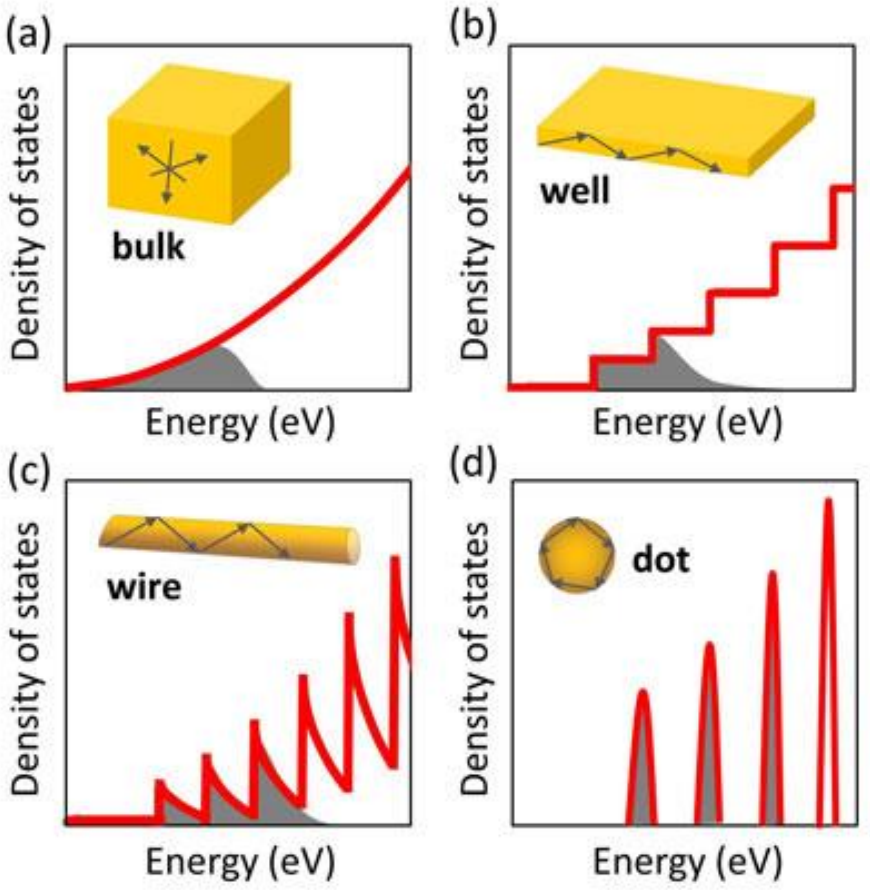

Figure 3 – Variation in density of states and their energy with particle shape

1.3. CdSe Quantum dots

The most famous and well-studied type of quantum dots are cadmium-selenide (CdSe) QDs.[7,8] These are semiconductor nanocrystals composed of a CdSe core and a ligand shell. Ligands play important roles in the stability and solubility of these nanoparticles. During synthesis, ligands stabilize growth to prevent aggregation and precipitation of the nanocrystals. These capping ligands also affect the quantum dots electronic and optical properties by passivating surface electronic states.[9]

To improve fluorescence quantum yield (QY), quantum dots can be made with "shells" of a larger bandgap semiconductor material around them, like CdS. The improvement is suggested to be due to the reduced access of electron and hole to non-radiative surface recombination pathways in some cases, but also due to reduced auger recombination in others.[10]

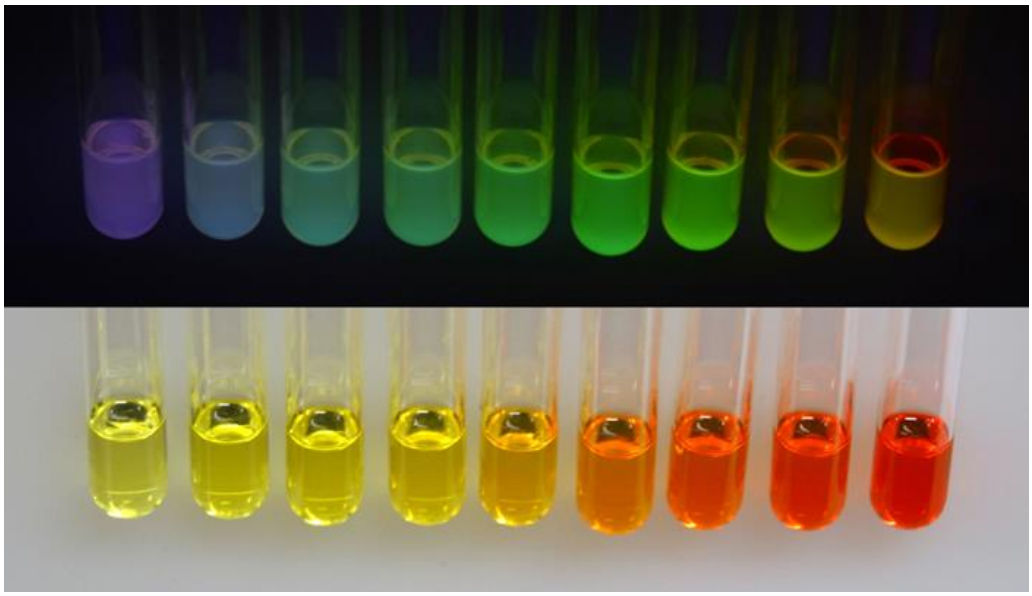

Figure 4 – CdSe Quantum dots under UV light (top) and daylight (bottom) with different sizes, growing from left to right

CdSe quantum dots have been implemented in a wide range of applications including solar cells[11], light emitting diodes[10], and biofluorescent tagging.[12] CdSe-based materials also have potential uses in biomedical imaging.[13] However, semiconductor quantum dots have certain limitations, with the most concerning being their toxicity due to the use of heavy metals in their production. Even after coated with several shells of non-toxic materials it is difficult to guarantee no leakage of cadmium ions or other toxic metals.[14]

1.4. Carbon dots

Carbon dots (CDs), also called carbon nanoparticles (CNPs), are one emerging new type of material that have shown great potential. They were first obtained accidently by Xu *et al.* in 2004 during the purification of single-walled carbon nanotubes (sw-CNTs) through preparative electrophoresis.[15] In 2006 Sun *et al.* reported the synthesis of this type of material via laser ablation of graphite powder, he was also the first to use the term "carbon quantum dots" (CQDs) to define these fluorescent carbon nanoparticles.[16]

CDs are normally divided into graphene quantum dots (GQDs), carbon quantum dots (CQDs) and polymer dots (PDs). The main difference between these types of carbon materials is their structure: GQDs have a single layer carbon (graphene) core with connected chemical groups on the surface or edge[17]; PDs possess aggregated polymer structures[18]; and CQDs, sometimes also referred to as carbon nanodots (CNDs), comprise all other types of carbon nanoparticles.

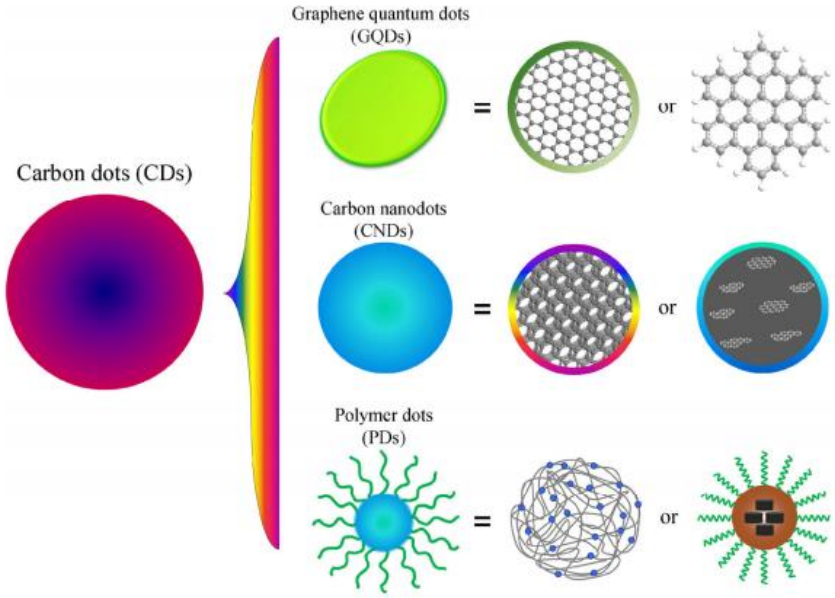

Figure 5 – Schematic illustration of different types of CDs

Contrary to traditional quantum dots, these type of material are not made of semiconductor materials but instead small organic molecules condensed together to form nanoparticles (< 10nm). [19,20]

Despite their different nature, CDs exhibit similar properties to semiconductor QDs, i.e. high fluorescence intensity and resistance to photobleaching. In addition to having similar fluorescence properties, CDs also have low toxicity,

biocompatibility, low cost and chemical inertness, which makes them very attractive for several applications.[20,21]

There are, however, some difficulties to overcome before CDs can really replace traditional semiconductors QDs, among them are the complex procedures for their separation, purification and functionalization, their generally low quantum yields, and ambiguity in their geometry, composition and structure.

A wide variety of methods have been used to synthesize CQDs, which can be classified into "top-down" and "bottom-up".

Figure 6 – Schematic illustration of CDs preparation via "top-down" and "bottom-up"

Top-Down methods typically involve the cleavage of bulk materials like graphene sheets, graphite particles, carbon nanotubes and nanodiamonds, followed by surface passivation of the as prepared CDs. Most used top-down methods are laser ablation[22], electrochemical carbonization[23] and arc discharge.[24]

Bottom-Up methods consist in assembling CDs from small organic molecules like citric acid, EDTA or some alcohols, also followed by surface passivation. Examples of this type of synthetic methods are hydrothermal treatment[25], microwave irradiation[26] and size control-confined pyrolysis.[27]

Although many new synthetic methods of preparing CDs have emerged in recent years, there are still some room to improving, namely in the size control, aggregation prevention and surface proprieties.

Size control and uniformity are one of the main challenges in CDs synthesis, it is important to guarantee uniform proprieties. Several ways of overcoming this challenge were reported, but the most commonly used are the employ of stabilizing agents and surfactants during synthesis. It is also possible to optimize size dispersion via post-treatment, such as gel electrophoresis, centrifugation, filtration, column chromatography and dialysis.

1.5. Carbon dots photoluminescence

Most CDs exhibit PL, however, the origin of this PL is not always clear and is still open for debate within the scientific community.

Four different types of emissive states have been confirmed (i) carbon core states; (ii) surface states; (iii) molecule states; and (iv) states formed by the cross-link enhanced emission (CEE) effect.[18,28]

The carbon core state is caused by the quantum confinement effect of conjugated π-domains determined by the carbon core. As mention before, this effect occurs when quantum dots are smaller than their exciton Bohr radius. This is thought to be the true intrinsic PL centre in GQDs since they have a perfect graphene core and less surface chemical groups. This PL emission can be tuned by the size of the conjugated π-domains i.e. the GQD.

The surface state (also called defect state) arises from the functional groups present at CDs surface. These functional groups have various energy levels, which may result in a series of emissive traps. In CQDs, a higher degree of surface oxidation or other effective modification can result in more surface defects, resulting in a red-shifted emission, which supports the theory that in CQDs the emission is dominated by the surface state emissive traps. These surface states do not consist of isolated chemical groups but rather the hybridization of the carbon backbone and connected chemical groups.

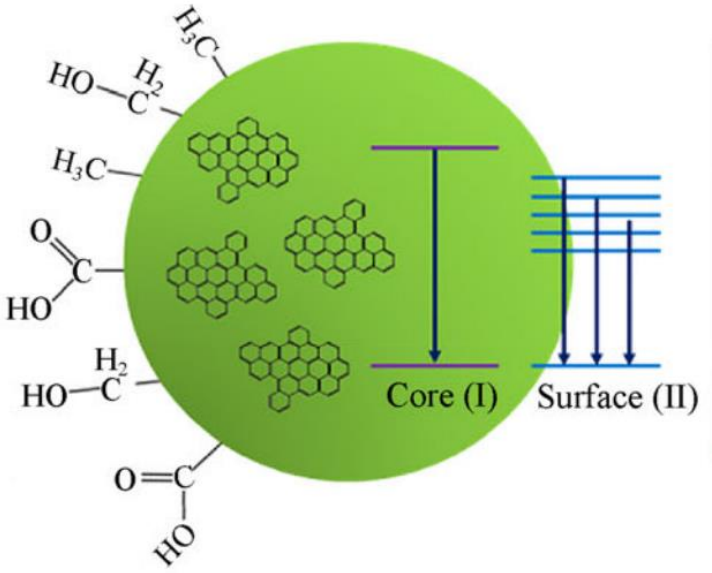

Figure 7 – Schematic illustration of core and surface-state emission

At first glance, molecule and surface state seems to refer to the same thing, however, the two should not be confused. As mention above, the surface state is the PL centre, formed by the synergetic hybridization of the chemical groups and the carbon core, whereas the molecule state is the PL centre formed solely by an organic fluorophore; the fluorophore is connected on the surface or interior of the carbon backbone and can exhibit PL emission directly. These organic fluorophores are formed in the first stages of CDs formation, at low reaction temperatures, and then as the carbonization temperature increases, the carbon core is formed by dehydration of the initial molecules or consumption of the formed fluorophores.

The molecule state is the emerging PL centre for a CDs prepared by small-molecule carbonization, like CQDs. These CDs typically exhibit strong PL emission with high QYs, whereas the carbon-core state possesses weak PL behaviour with high photostability.

In PDs, owing to the crosslinked skeleton, the vibration and rotation of the amino-based fluorophores is restricted, and the percentage of radiative processes increased (CEE effect). These PDs exhibit temperature-dependent PL, higher temperatures aggravate the vibration and rotation, thus increasing the non-radiative process.

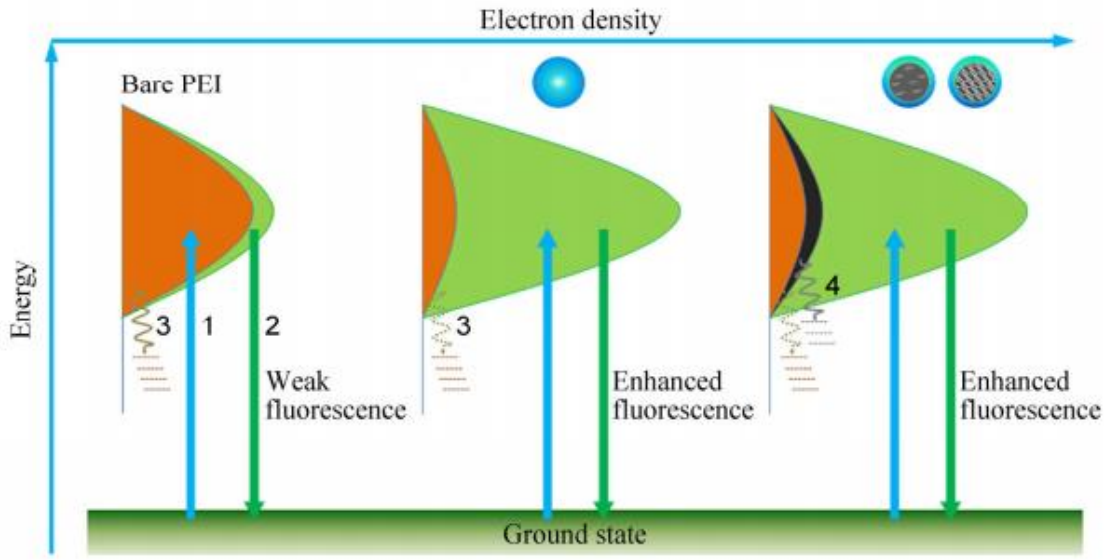

Figure 8 – Representation of PDs PL mechanism (CEE effect)

1.6. Carbon quantum dots functionalization

After synthesis, it is possible to tune and improve CQDs properties through surface modification. There are many approaches for functionalizing the surface of CQDs, like covalent bonding, coordination, π–π interactions, and sol–gel technology. [9,16,19]

Most CQDs are rich in functional groups, like carboxylic acids, ketones, esters, and amines, which makes them suitable for covalent bonding. Surface passivation via covalent bonding of carboxyl-containing agents is a common method to improve the PL of CQDs, which showed an important influence on the properties of CQDs. [29]

Carbodiimide compounds provide the most popular and versatile method for crosslinking amines to carboxylic acids. The most readily available and commonly used carbodiimides are the water-soluble EDC for aqueous crosslinking and the water-insoluble DCC for non-aqueous organic synthesis methods.

Carbodiimide conjugation works by activating carboxyl groups for direct reaction with primary amines via amide bond formation. Because no portion of their chemical structure becomes part of the final bond between conjugated molecules, carbodiimides are considered zero-length carboxyl-to-amine crosslinkers.

N-hydroxysuccinimide (NHS) is often included in EDC coupling protocols to improve efficiency and/or create dry-stable (amine-reactive) intermediates. EDC couples NHS to carboxyls, forming an NHS ester that is considerably more stable than the O-acylisourea intermediate while allowing for efficient conjugation to primary amines.

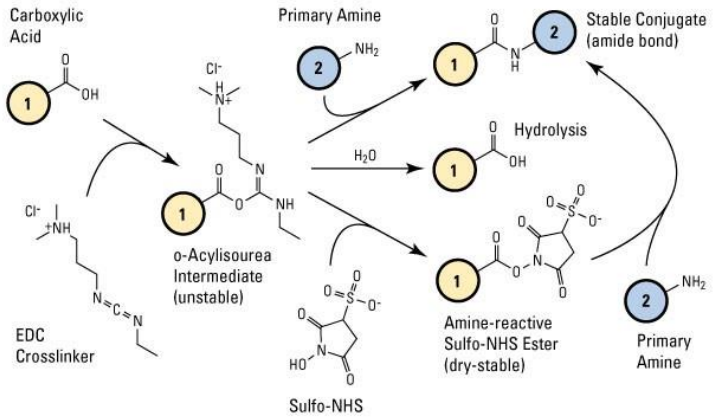

Scheme 1 – Crosslinking chemistry using EDC and NHS

1.7. Functionalization of CQDs with spiropyran

Liao *et al.* reported the functionalization of CQDs, obtained by hydrothermal carbonization of EDTA, with spiropyrans.[29] The emission of the functionalized CQDs centred at 510 nm could be switched off, while being turned on at 650 nm via energy transfer between the CQDs and spiropyrans after irradiation with ultraviolet (UV) light. The process could be reversed using irradiation with visible light. The functionalized CQDs show excellent photo-reversibility and high stability.

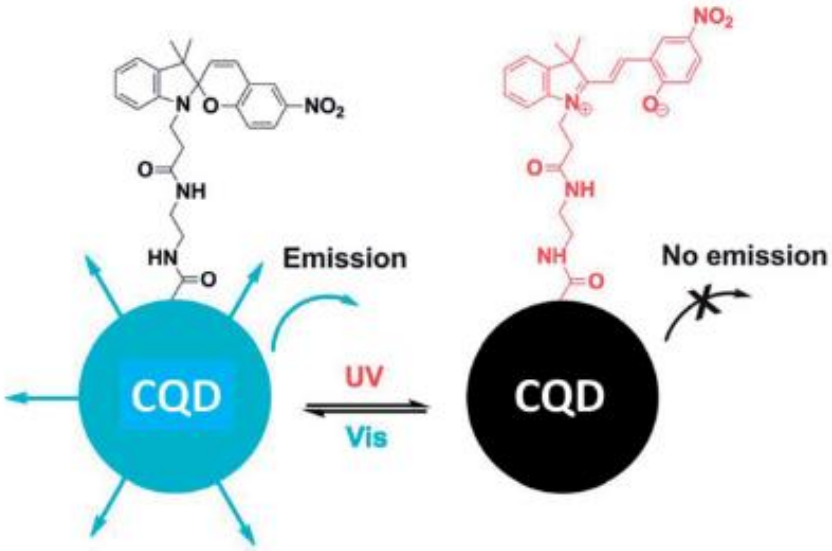

Scheme 2 - Schematic illustration of light-induced fluorescence modulation of the spiropyran-functionalized CNPs

1.8. Carbon dots doping

Doping is a widely-used approach to tune the PL properties of photoluminescent materials. Various doping methods with dozens of elements such as N, S, and P have been reported to tune the properties of CQDs.[30,31] N-doping is the most studied way to enhance the emission of the CQDs by inducing an upward shift in the Fermi level and electrons in the conduction band.[31] It was demonstrated that only the nitrogen bonding to carbon can really enhance the PL emission of CQDs. The N-CQDs show nitrogen content-dependent PL intensities with multicolour and two-photon up-conversion properties.

1.9. Flavylium salts

Flavylium compounds are versatile molecules that can be found in nature in the form of anthocyanidins and anthocyanins, pigments that are responsible for the colours of many flowers.[32] Anthocyanidins are the sugar-free counterparts of anthocyanins, common plant pigments that may appear red, purple, or blue depending on the pH. Flavylium is the name given to the 2-phenylbenzopyrylium ion, a derivative of benzopyrylium with a phenyl group attached in position 2 (see Scheme 3).

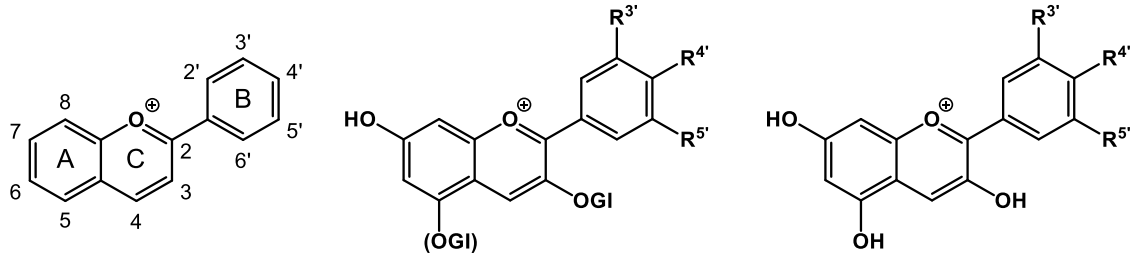

Scheme 3 – Structure of anthocyanin compounds and the flavylium cation (Gl = glycoside)

In solution flavylium salts can undergo various structural transformations that can be driven by pH changes or light excitation.[33,34] These transformations are normally accompanied by colour change or disappearance.

Under strongly acidic conditions the flavylium cation, **AH+**, is the stable form. When the pH is raised the flavylium cation can participate in two parallel reactions (i) deprotonation to form the quinoidal base **A**; (ii) hydration in position 2 followed by proton loss to give the hemiketal **B**. The quinoidal base is the kinetic product since proton transfer is faster than the hydration reaction but in many cases the thermodynamic product is the trans-chalcone (**Ct**). This means that **A** can be formed as a kinetic product, and later totally or partially disappears to yield the thermodynamic equilibrium. The trans-chalcone is formed by isomerization of cis-chalcone (**Cc**) that forms from **B** via a tautomeric ring-opening process.

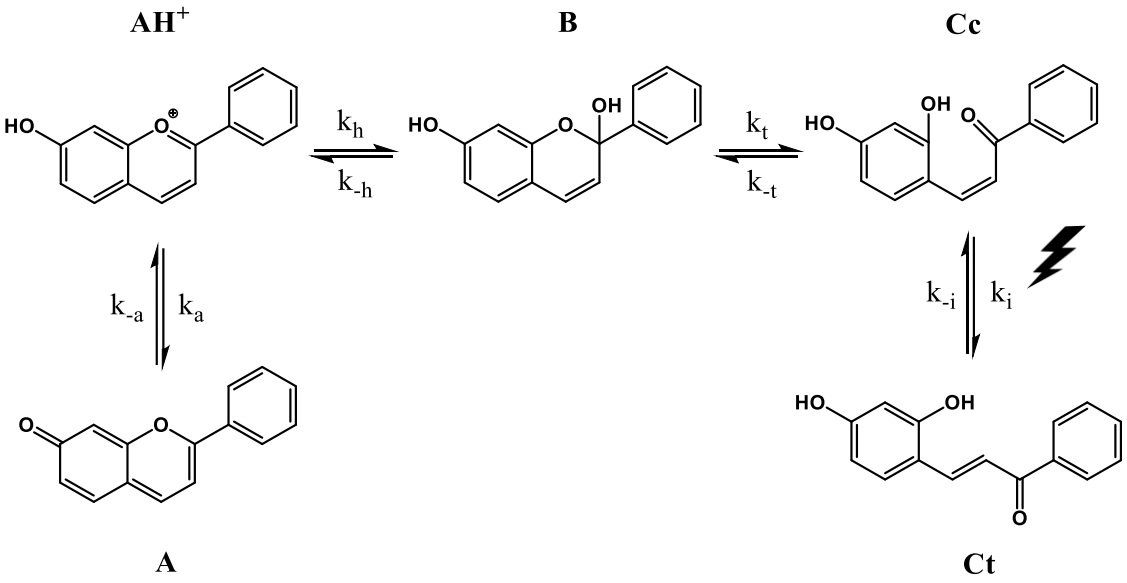

Scheme 4 – Flavylium network of chemical reactions

Something very interesting in this type of systems is that **AH**$^+$ and **B** can be interconverted by pH changes, while **Cc** and **Ct** can be interconverted by photo-excitation. In sufficient basic pH **Cc** and **Ct** can undergo deprotonation to give the **Cc**$^-$ and **Ct**$^-$ monoanions, respectively, which can also be interconverted by light excitation.[35]

At equilibrium, this system behaves as a single acid–base equilibrium between the flavylium cation and a conjugate base, CB, defined as the sum of the concentrations of the other species in the network, [CB] = [A] + [B] + [Cc] + [Ct].

The experimental work involved three distinct components (i) the synthesis of CQDs; (ii) the synthesis of flavylium salts containing a carboxyl tail; and (iii) the functionalization of CQDs with the synthesized flavylium salts. The results will, therefore, be presented in three separated chapters.

2

Carbon Quantum Dots (CQDs)

In this chapter it is discussed the synthesis and characterization of CQDs, following a method previous described by Sun *et al.*[31] The characterization was done by UV-vis absorption spectroscopy, steady-state and time-resolved fluorescence spectroscopy, and transmission electron microscopy (TEM).

The main goal was the synthesis of highly fluorescent CQDs using well defined starting materials (single molecules instead of complex organic matrixes like biomass), and with functional groups attached to their surface so that they can be easily functionalized.

1.1. Synthesis of CQDs

The synthesis of this QDs was accomplish by hydrothermal treatment of citric acid and Ethylenediamine (EDA) in water. The citric acid acts as a carbon source while the EDA acts as a basic catalyst and passivation agent.

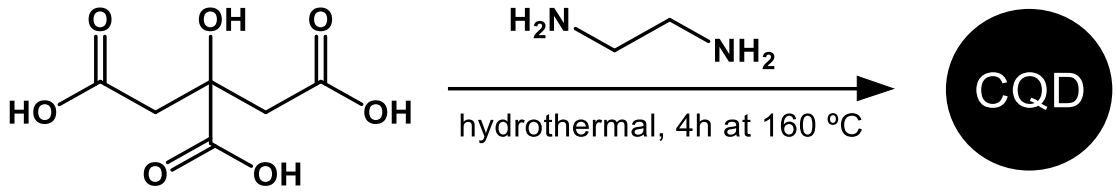

Scheme 5 – Hydrothermal reaction

The reaction conditions (temperature, reaction time and concentration of reagents) where already optimized by Sun *et al.*[31] Is was chosen the reactions conditions that yielded the higher fluorescence QY (94%).

Purification of the as-synthesized CQD is a critical step in the overall fabrication process. The presence of unreacted precursors or excess surfactants can limit charge transfer and decrease the fluorescence QY.

CQDs were purified by multiple cycles of precipitation with anhydrous ethanol followed by centrifugation and discard of the precipitate. The final step was the filtration of the supernatant using a nylon membrane with a pour opening of 200 nm.

It was also attempted to use dialysis was purification method, however, it was found that both CQDs and citric acid/EDA could pass through the membrane (1 kD). Some authors claim to use such a membrane to purify similar CQDs[29, 36], however in your case that was not possible. Because no membrane with a lower molecular weight cut-off (MWCO) was available, this purification method was abandoned.

Regarding the precipitation/centrifugation cycles, this method was also used by Sun *et al.*[31], in their case the supernatant was discarded and the CQDs were collected in the precipitate. In our case, the precipitate exhibited no fluorescence, even after re-dispersed in water. By contrast, the supernatant fluorescence remained the same (or even higher). This is further discussed in 1.3.

1.2. Study of CQDs optical properties

The absorption spectrum shows strong absorption bands in the UV region with a tail extending to the visible region. The absorption shoulder at 250 nm correspond to π – π* transition of the carbon core. Another absorption shoulder appears at 355 nm corresponding to n – π* transition of the surface functionalized C=O bonds or other connected groups.

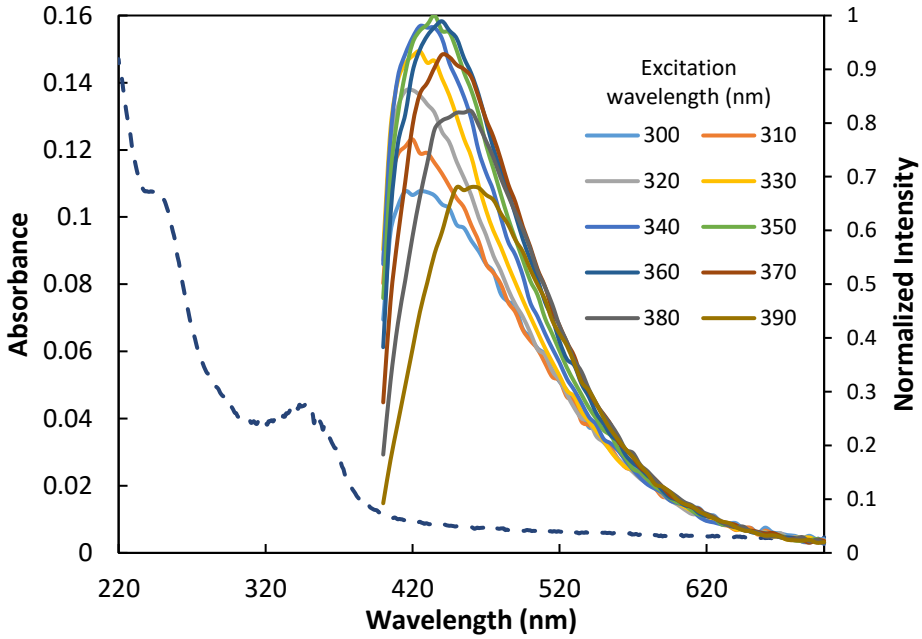

Figure 9 – UV-Vis spectra (dashed line) and PL emission spectra (solid lines) as a function of excitation wavelength

CQDs exhibit a wide emission peak wide with large stocks shift (≈ 6349 cm^{-1}) when compared with that of organic dyes. This emission peak seems to be excitation wavelength-dependent, which means that the emission maxima changes with the excitation wavelength. This may result from the wide distributions of differently sized dots and surface chemistry.

By exciting at the optimal excitation wavelength (350 nm), the strongest emission peak is observed at 450 nm. This emission maximum then shifts towards higher wavelengths with increasing in the excitation wavelength. In the excitation spectra below (Figure 10) it is possible to see this shift, as well as evidence of a second excitation band in the UV region (< 270 nm).

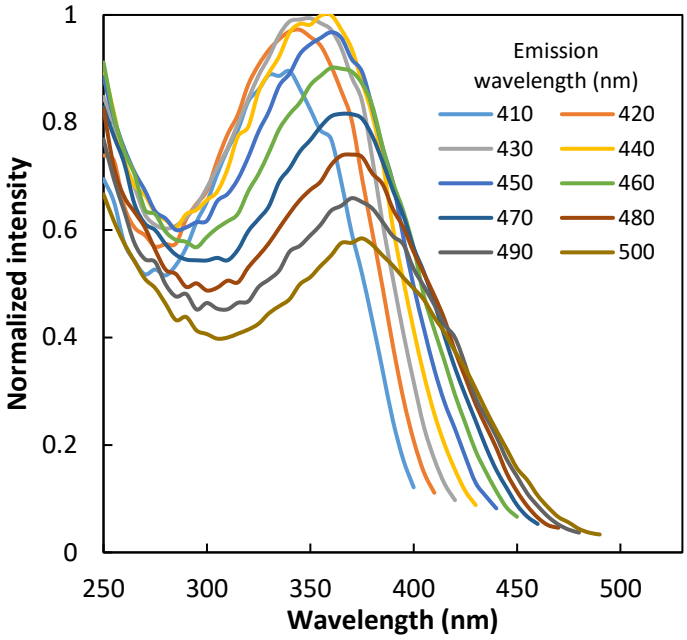

Figure 10 – PL excitation spectra of CQDs collecting at different wavelengths

The longer wavelength excitation band (290 – 470 nm) can be attributed to surface defects or states and it is referred to as the S-band. The second excitation band observed at the lower wavelength region (< 270 nm) can be attributed to the π–π* transition of the carbon core and it is referred to as the C-band.

It is observed that the S-band shows relatively broad absorption (285–470 nm) and a continuous shift in its excitation maximum relative to the monitoring wavelength. This is an indication that the different surface states, due to CQDs surface heterogeneity, are responsible for the observed excitation-dependent emission maximum.

Figure 11 shows a side-by-side comparison of CQDs emission, exciting the C-band (240 – 270 nm) and the S-band (340 – 390 nm). Unfortunately, our spectrofluorimeter is unable to irradiate samples below 240 nm (the lamp correction file was generated above 240 nm), so it was not possible to fully characterized the C-band, however, the acquired data showed no shift on the emission band, which indicates that the π–π* transition of the carbon core has no influence on the excitation-dependent emission behaviour.

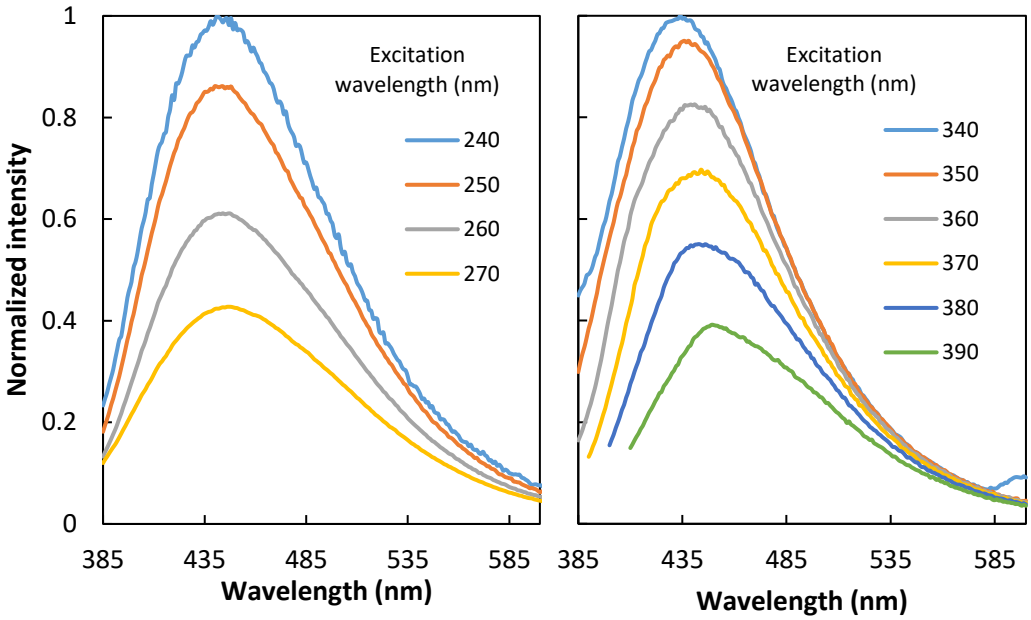

Figure 11 – PL emission spectra, exciting the C-band (left) and the S-band (right)

The 3D fluorescence spectra (Figure 12) show two distinct contours (corresponding to C-band and S-band) of almost equal intensity appearing at the same emission maximum (450 nm), i.e., excitation of the C-band or the S-band lead to the same PL maximum. This clearly indicates that, even when the excitons are generated at the carbon core, they get trapped and relax at the surface defects before recombination, this explains why both bands have the same emission curve and the large stokes shifted observed.

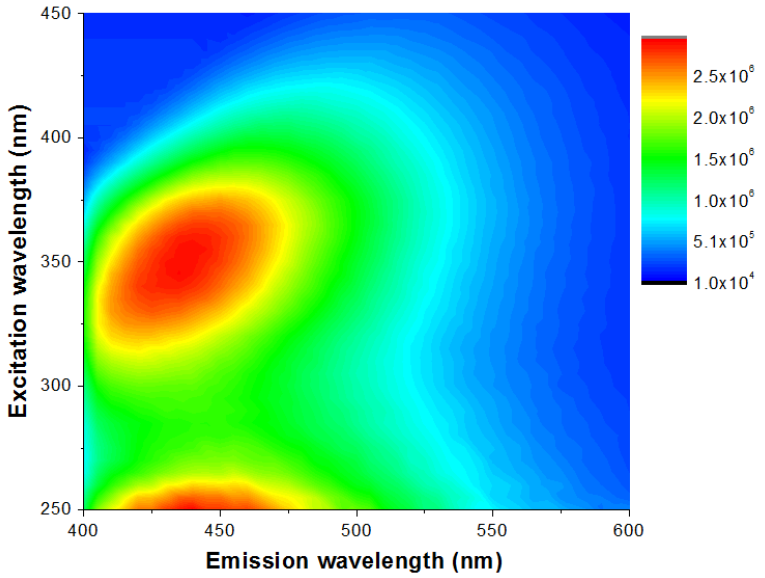

Figure 12 – 3D fluorescence spectra of CQDs

1.3. Study of the influence of precipitation/centrifugation cycles on CQDs optical properties

In order to determine the ideal number of precipitation/centrifugation cycles, CQDs from the same batch were subjected to the same purification steps, varying the number of purification/centrifugation cycles.

The as purified CQDs were then dried in a rotary evaporator and re-dispersed in water at pH 5 (as seen before, there is no significant variation of PL intensity or fluorescence QY around this pH value, which eliminates the need to correct small changes in pH). The absorbance values of these solutions were adjusted to roughly 0.1 and the PL spectra was obtained. Fluorescence QY was calculated by the relative method using 8-Anilinonaphthalene-1-sulfonic acid (ANS) as standard.

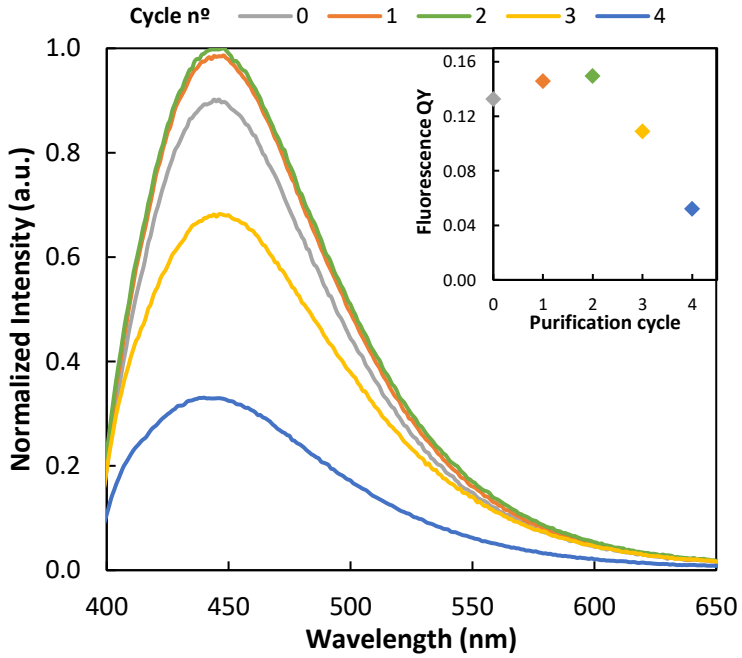

Figure 13 – PL spectra and fluorescence QY (Inset) as a function of purification cycles (λ_{ex} =360 nm)

Figure 13 shows that the first two purification/centrifugation cycles led to a slight increase in PL intensity (≈11%) and QY (≈13%), however following cycles drastically diminished PL intensity (≈64%) and QY (≈61%). This can be explained by the loss of ligands attached to CQDs surface, which interfere with the surface states responsible for PL.

1.4. Study of pH influence on CQDs optical properties

Since flavylium salts are pH-sensitive, it was also important to determine how pH changes influence CQDs optical properties like absorbance and PL.

This was done by preparing a stock solution of CQDs in water at pH 1 and then transferring 1 mL to several plastic cuvettes. In each cuvette 1 mL of NaOH 1 M was added and 1 mL of phosphate buffer with the desired pH value. Absorbance, fluorescence emission and excitation spectra of each sample were recorded, and the fluorescence QY was later calculated using the same method as before.

Perchloric acid ($HClO_4$) was used to adjust the buffer pH instead of hydrochloric acid (HCl) because in very acidic conditions (pH < 2) Cl^- ions can quench fluorescence.

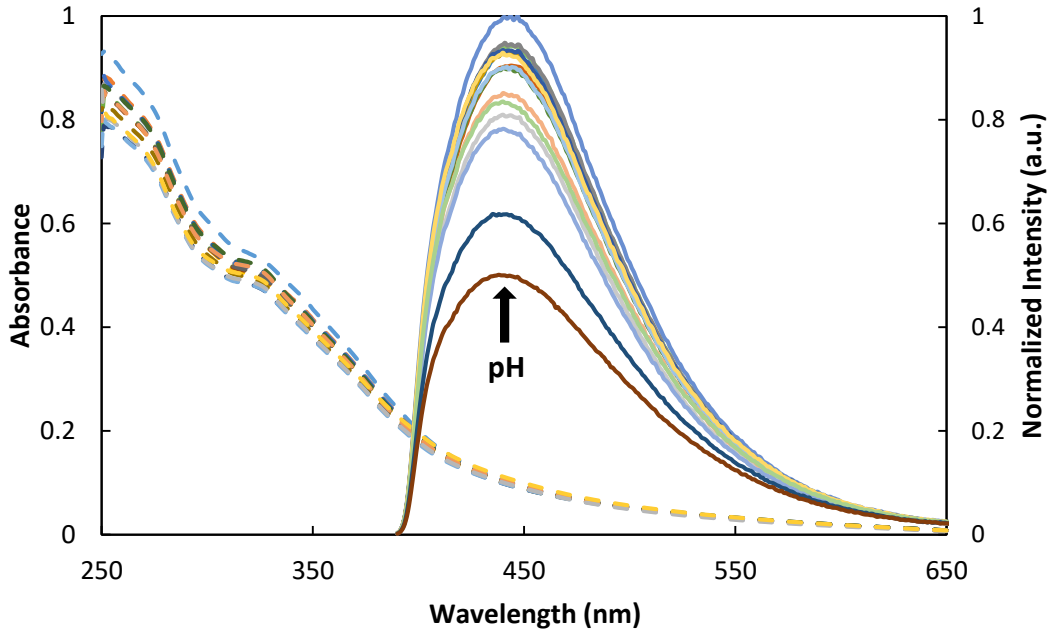

Figure 14 – UV-Vis spectra (dashed lines) and PL spectra (solid lines) as a function of pH, from pH 1.2 to pH 7 (λ_{ex} = 360 nm)

As shown in the above chart, although no significant change was possible to observe in the absorbance spectra, there is a clear dependence of PL with the pH value. This can be explained by the protonation and deprotonation of surface oxygen-containing groups, responsible for oxygen-related surface states where luminescence originates. This protonation and deprotonation can also cause electrostatic doping/charging of the CQDs, which can also influence the PL.

Figure 14 shows that the PL intensity of CQDs increased drastically (≈102%) as the pH increased from 1.2–7. A similar behaviour was observed for the fluorescence QY (Figure 15), which increased significantly (≈57%) as the pH increased, however, after pH 3 there was almost no variation of QY.

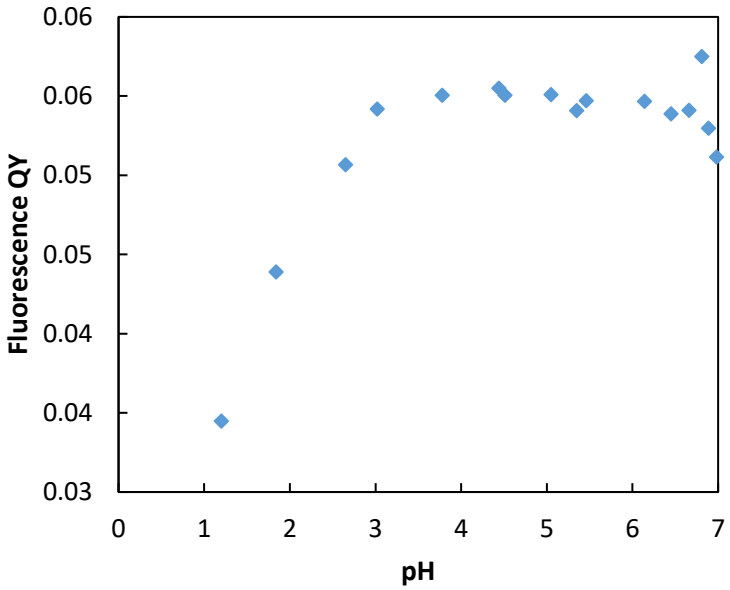

Figure 15 – Fluorescence QY as a function of pH, from pH 1.2 to pH 7 (λ_{ex} = 360 nm)

1.5. Fluorescence lifetime measurements

Fluorescence lifetime measurements were made in a custom single photon counting (SPC) apparatus, irradiating a solution of CQDs with a pulsed LED (λ_{ex}=370 nm) and collecting the emitted photons at three different wavelengths: 430, 450, and 470 nm. Measurements were also made at four different pH values.

Fluorescence lifetime were calculated by making a global fit of the three decays collected at different wavelengths, for each pH value (Figure 16, left). All samples exhibited double exponential lifetime decay, indicating that fluorescence may originate from two different species.

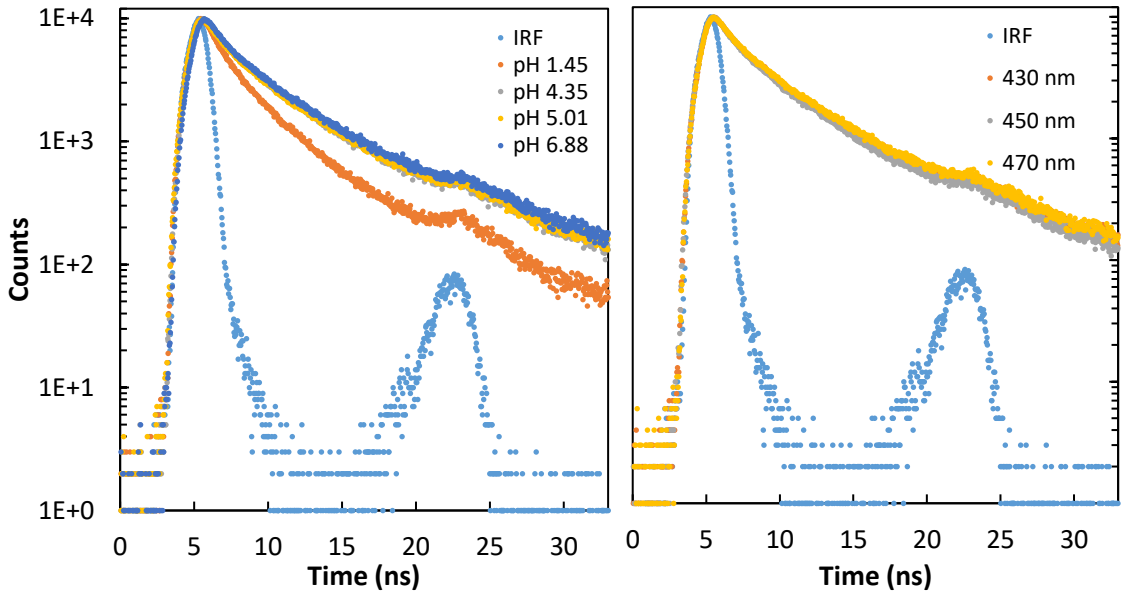

Figure 16 – Fluorescence lifetime decays collected at 450nm (left) as a function of pH, and at pH 5.01 (right) as a function of collected wavelength

The calculated mean fluorescence lifetimes are greater at higher pH values, i.e., the fluorescence intensity decays at shorter timescale in the lower pH values and at longer timescale in the higher pH range (Table 1).

At the same pH value (exciting at 370 nm) there is no considerable variation in the fluorescence lifetime decay while monitoring at the different emission wavelengths (Figure 16, right). This indicate that the longer wavelength excitation selectively excites only the relaxed state/surface state.

Table 1 – Fluorescence lifetime measurements

pH	τ_1 (ns)	τ_2 (ns)	τ_{av} (ns)	$\chi 2$
1.45	2.932	8.570	4.304	1.192
5.01	2.992	8.427	5.373	1.118
6.88	2.902	9.062	5.388	1.174

1.6. TEM measurements of QCDs

TEM microscopy was fundamental to confirm the formation of CQDs and to assess the particle uniformity and size distribution. The measurements shown great uniformity with sizes ranging from 2.2 to 2.4 nm in diameter. Because the sample was too diluted, and CQDs are so small, it was only possible to observe a few CQD at a time. However, there was no sign of CQDs aggregation, which can happen in more concentrated solutions.

In more powerful TEM, like high resolution TEM (HR-TEM), it is even possible to measure the lattice fringes, which can be used to determine the crystal structure of the carbon cores.

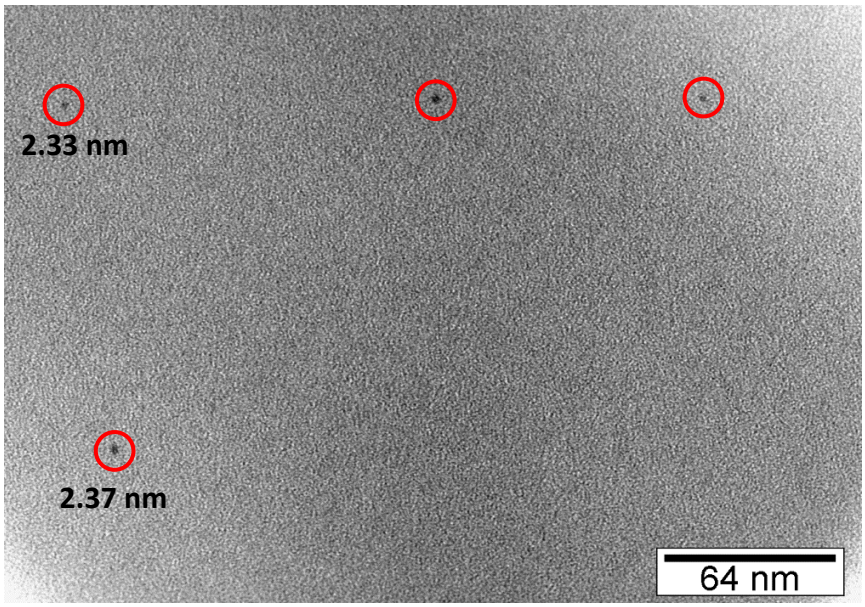

Figure 17 – TEM image of CQDs

3

Flavylium Salts

In this chapter, it is discussed the various attempts to synthesize flavylium salts suitable for CQDs functionalization, and their characterization. The main goal was the incorporation of a carboxylic tail in the flavylium skeleton in order to attach it to primary amines present at CQDs surface.

The first synthetic approach was based in a strategy proposed by Katritzky *et al*[37]. This strategy consists in synthesizing a flavylium salt and then attach it a molecule containing a carboxylic acid, at position 4.

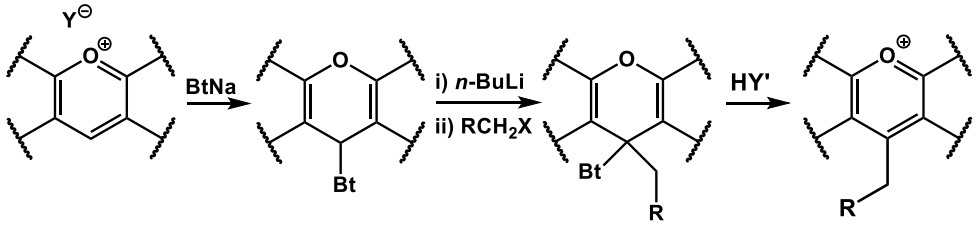

Scheme 6 – Engineering of benzopyrylium salts by indirect electrophilic substitution

The second synthetic approach was based in a strategy proposed by Robinson and Walker[38]. In this strategy the carboxylic tail is incorporated in an α,β–unsaturated ketone, which then react with a phenol to form a flavylium salt with the carboxylic tail in position 4'.

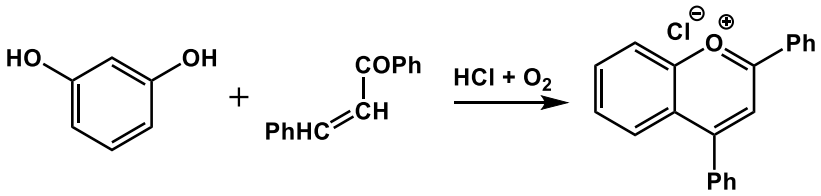

Scheme 7 – Condensation between phenol and unsaturated ketone in acidic conditions

1.1. Synthesis of 4'-metoxyflavylium (1)

The first step in synthesizing flavylium cations suitable for CQD functionalization was the synthesis of simple and well-studied flavylium. The chosen flavylium was the 4'-metoxyflavylium, since its reported absorption maximum is 450 nm, the emission maximum of CQDs. The synthesis was done following a method previously reported by Robinson and Walker[38], through the condensation reaction between a salicylaldehyde and an acetophenone in acidic medium.

Tetrafluorboronic acid (HBF_4) was used because the tetrafluoroborate anion (BF_4^-) makes the flavylium salts more soluble in organic solvents, needed for further steps. Furthermore, BF4− is less nucleophilic and basic than nitrates and halides. BF4− owes its inertness to its symmetry, the negative charge is distributed equally over four atoms, and it is composed of highly electronegative fluorine atoms, which diminish the basicity of the anion.

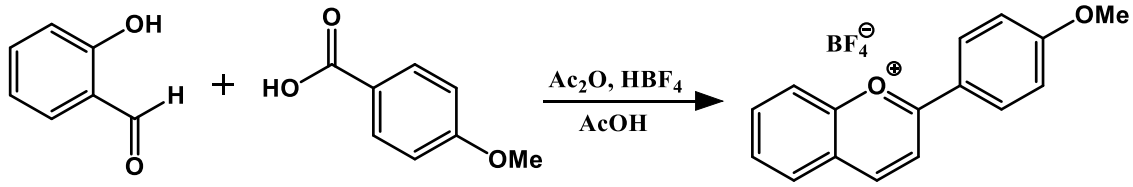

Scheme 8 – Condensation reaction between salicylaldehyde and an acetophenone

The reaction yields were in the range 30-40%. This low yield is due to the difficulty in precipitating the flavylium salt, which is more soluble in organic solvents due to the reasons stated above.

After the initial precipitation with diethyl ether (yielding a bright orange powder), the remaining dark solution was dried in the rotary evaporator and redissolved in a small amount of acetic acid. This solution was then frozen with liquid nitrogen (-195.79 °C) and a small amount of diethyl ether was added. After reaching room temperature it was possible to collect more flavylium salt by filtration.

The rapid drop of temperature induced flavylium precipitation, although, the obtained powder exhibited a dark orange colour, indicating that some impurities were still present. Even after further washings with chilled diethyl ether the powder remained dark orange. It was concluded that the rapid cooling induced

the precipitation of more flavylium salt but also allowed some impurities to become trapped in the crystalline structure. For this reason, only the first precipitated flavylium was used in the next reaction.

In both cases, the remaining acetic acid, a common impurity in flavylium synthesis, was removed by azeotropic distillation with toluene.

1.2. Synthesis of 4-benzotriazol-4'-metoxyflavylium (2)

In order to attach a carboxylic tail to the flavylium skeleton, necessary for CQDs functionalization, it was used a method previously reported by Katritzky *et al*[37]. This method consists of an benzotriazole-mediated indirect nucleophilic substitution in the position 4 (position *para* to the oxygen atom) of the flavylium.

The first step was the nucleophilic addition of benzotriazol at the position 4.

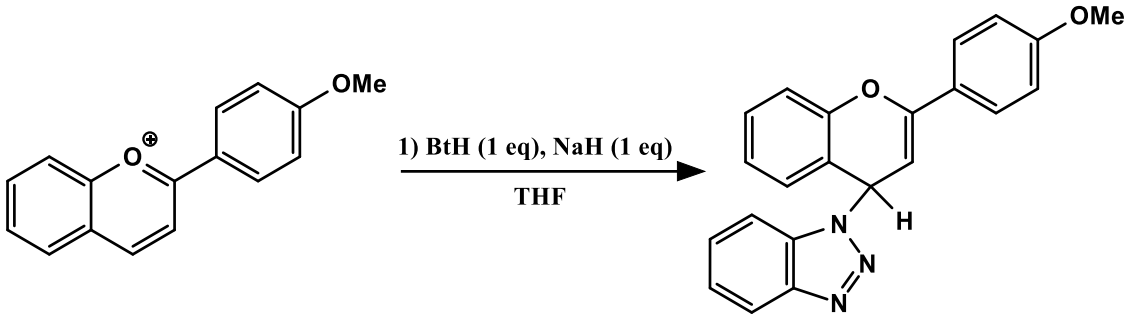

Scheme 9 – Nucleophilic addition of benzotriazole

Sodium benzotriazolate was generated in situ by deprotonation of the benzotriazole with sodium hydride (NaH), this reaction releases H_2 and was performed under a N_2 flow. When no more H_2 bubbles were observed (≈30 min) the previous synthesized 4'-metoxyflavylium was added and the solution stirred for another 30 min. Almost immediately after flavylium addition there was a loss of colour, something expected since the addition of benzotriazole at the position 4 breaks the conjugation in the system.

It is important to add only 1 equivalent of flavylium to the sodium benzotriazolate in order to guarantee a regiospecific *para* substitution and avoid the formation of ortho addition products. It is also important that when generating the sodium benzotriazolate both reagents are in stoichiometric quantities, if any NaH excess is present when the flavylium is added the deprotonation reaction may compete with the nucleophilic addition of benzotriazole.

1.3. Synthesis of 4-ethylacetate-4'-metoxyflavylium (3)

After attaching benzotriazole in the position 4, the ring reactivity is inverted and can now act as a nucleophile. For this to happen it is first necessary to remove the proton in position 4, which is now the more acidic proton due to the inductive effect of the benzotriazole group. This proton can be removed using a strong base like n-Butyllithium, forming a carbanion that can react with an electrophile like alkyl bromides.

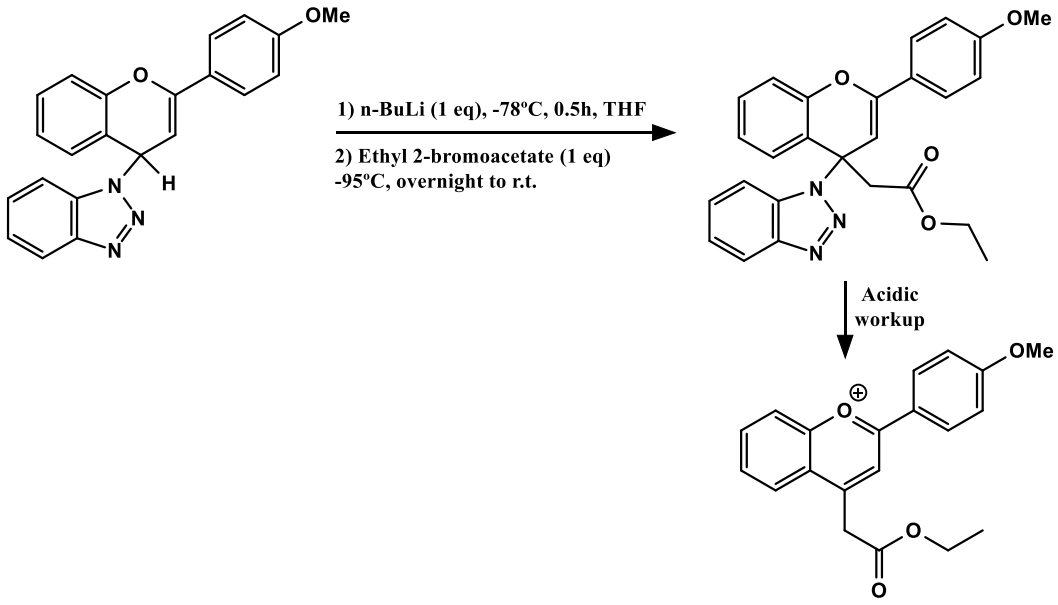

Scheme 10 – Electrophilic substitution followed by acid-promoted debenzotriazolylation and ester hydrolyze

The deprotonation reaction with n-BuLi must be done at very low temperatures (-95 °C) in order to stabilize the carbanion formed and to avoid a violent reaction. This low temperature can be achieved using a freezing bath of acetone. It is also important to use oven-dried glassware and a dry N_2 flow, in order to avoid side-reactions with water. To selectively remove the proton in carbon 4, only one equivalent of n-BuLi must be added or other protons will also be removed. The formation of the carbanion can be seen as the solution regain colour

(deep blue). This is typical of carbanions and is a good indicator of the deprotonation reaction.

After addition of the electrophile, ethyl 2-bromoacetate, the reaction follows a SN_2 mechanism, with the leaving group Br- being substituted by the 4-benzotriazol-4'-metoxyflavylium. This is again accompanied by a colour change (deep blue to bright orange)

Figure 18 – Reaction mixture before (left) and after (right) electrophile addition

The last step in this reaction is the acid-promoted debenzotriazolylation, achieved by the addition of diluted acetic and perchloric acid. The addition of these acids also promotes the hydrolysis of the acetate group, yielding the carboxylic acid.

Unfortunately, the final compound was not stable in aqueous solution and suffered degradation, forming a green amorphous film.

1.4. Synthesis of 4-(bromomethyl)acetophenone (4)

The first step in this synthetic route was the bromination of 4-methylacetophenone using the Wohl-Ziegler reaction, this reaction follows a radical pathway and allows to selectively bromate benzylic C-H bonds.

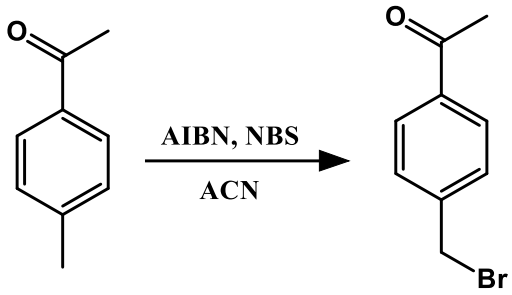

Scheme 11 – Wohl-Ziegler bromination reaction

It is very important to keep the concentration of Br_2 and HBr low to prevent side reactions. These reagents are therefore generated in situ from N-bromosuccinimide (NBS). To kick-start the reaction a radical initiator is used: Azobisisobutyronitrile (AIBN).

When heated, AIBN decomposes eliminating a molecule of nitrogen gas to form two 2-cyanoprop-2-yl radicals:

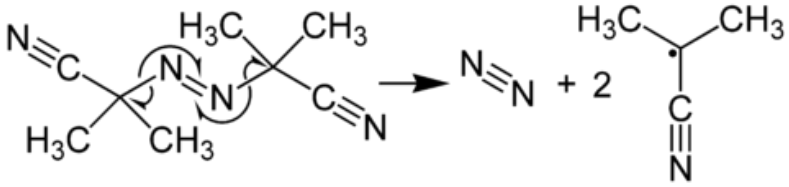

Scheme 12 – Decomposition of AIBN

It is important that the NBS sample have already some Br_2 present to start the reaction. Pure NBS have a white colour but with time and/or moisture it starts to become yellow, this is an indication of Br_2 presence and it is preferable to use such sample.

In the initiation step of this reaction, the 2-cyanoprop-2-yl radicals react with Br_2 molecules to generate Br radicals.

Scheme 13 – Initiation step

The propagation reaction can be divided in two steps: (i) first the bromine radical breaks the C-H bond, forming the benzylic radical and HBr (ii) then the benzylic radical attacks Br_2 to re-generate bromine radical.

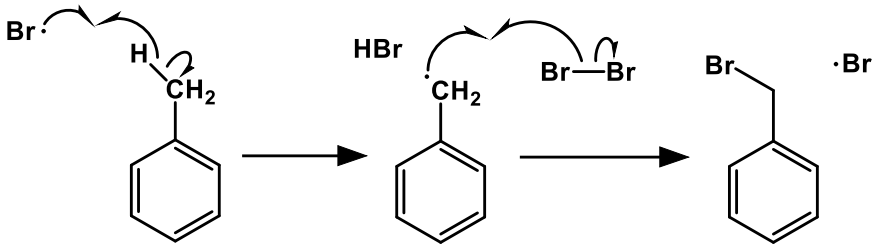

Scheme 14 – Propagation steps

After the initial Br_2 molecules are consumed, Br_2 starts to be generated from the reaction between HBr and NBS.

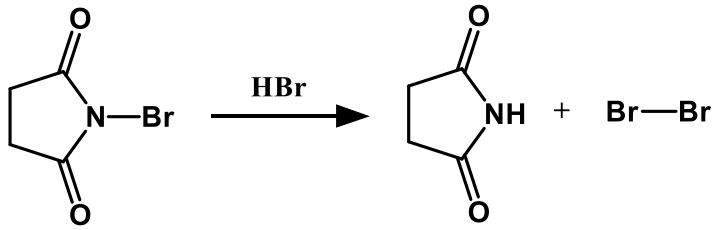

Scheme 15 – Generation of Br_2 from NBS

Since one equivalent of HBr generates one equivalent of Br_2, bromide will be generated only after the completion of the first propagation step, this keeps the concentration of Br_2 low.

NBS is poorly soluble in acetonitrile and the resulting succinimide is insoluble and floats to the surface. This keeps the concentration of reagents low and is a signal that the reaction is finished.

Most by-products can be separated from the final product by dissolving in toluene and discarding the precipitate. Further purification is done by silica gel column chromatography.

1.5. Synthesis of (4-Acetylphenyl)acetonitrile (5)

After the bromination reaction the bromine was exchanged with a cyanide group, making a new C-C bond. This reaction is a simple nucleophilic substitution.

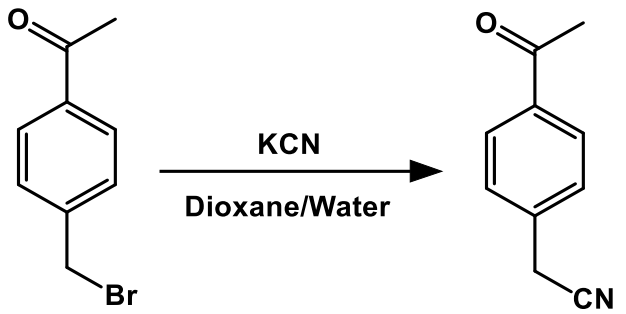

Scheme 16 – Nucleophilic substitution of Br for CN

Although being a simple reaction, it is a very dangerous one due to the formation of hydrogen cyanide, a colourless, extremely poisonous and flammable liquid that boils slightly above room temperature.

One way to minimize the risk of working with cyanide, is to perform the reaction in a closed apparatus, with a gas outlet connected to a trap containing an alkaline solution of potassium permanganate. In this way, any HCN gas that escapes the reaction vessel, must first pass through the potassium permanganate solution, were it is oxidized to potassium cyanate, a much safer to handle salt.

The final product was again purified by silica gel column chromatography.

1.6. Synthesis of (4-Acetylphenyl)acetic acid (6)

The last step was the transformation of the nitrile group into a carboxylic acid, this was done by acid catalysed hydrolysis.

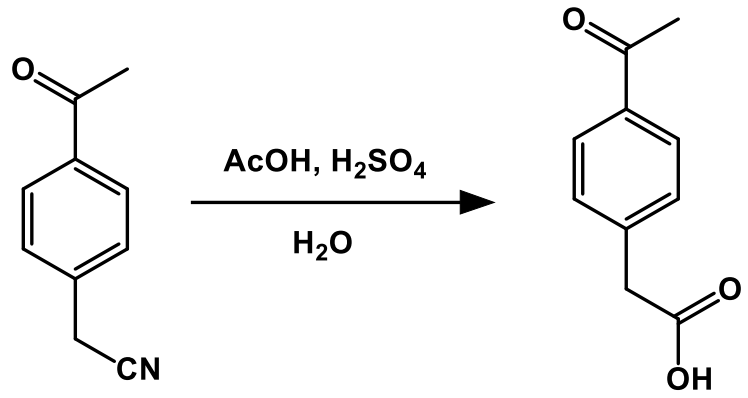

Scheme 17 – Acid catalysed hydrolysis reaction

The nitrile was first hydrolysed to amide, followed by another hydrolyse to yield the carboxylic acid. After extraction with ethyl acetate, the final product was isolated as a white crystal

1.7. Synthesis of 4'-methylcarboxyflavylium (7)

Using the acetophenone (6), it was synthesized a flavylium salt by a simple condensation reaction with 2-hidroxybenzaldehyde, as described for compound (1).

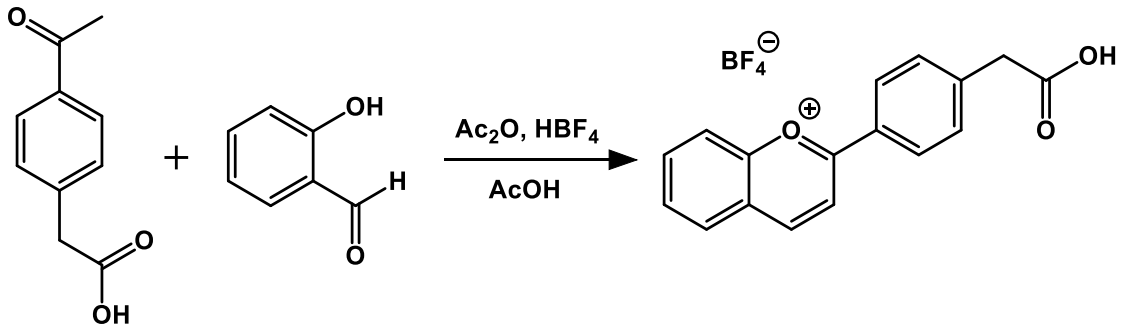

Scheme 18 – Condensation reaction of (4-Acetylphenyl)acetic acid with 2-hidroxybenzaldehyde

This flavylium salt was also precipitated with ethyl ether, with a reaction yield of almost 80%.

Despite the reaction high yield, the flavylium proved to be unstable in solution, almost immediately after being dissolved in water a green precipitate was observed. This precipitate was collected and re-dissolved in deuterated chloroform, in an attempt to make the NMR spectra of this compound. (See section 3.14)

1.8. Synthesis of 7-hydroxy-4'-methylcarboxyflavylium (8)

In order to synthesize a more stable flavylium, the previous reaction was repeated using 2,4-dihydroxybenzaldehyde. This allowed for the integration of a hydroxyl group in the position 7.

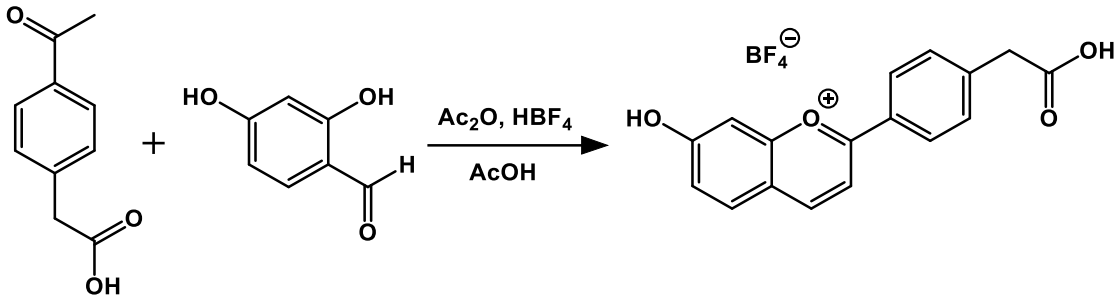

Scheme 19 – Condensation reaction of (4-Acetylphenyl)acetic acid with 2,4-hidroxybenzaldehyde

The final flavylium was precipitated as described before, but with a lower yield: 38%. The compound structure was confirmed by NMR, elemental analysis and mass spectroscopy (ESI/MS). This flavylium was then used to functionalize CQDs.

Table 2 – Elemental analysis of 7-hydroxy-4'-methylcarboxyflavylium

Formula: $C_{23}H_{17}ClO_4 \cdot H_2O$	
Calculated	**Determined**
C: 52.88	C: 52.64
H: 3.92	H: 4.12

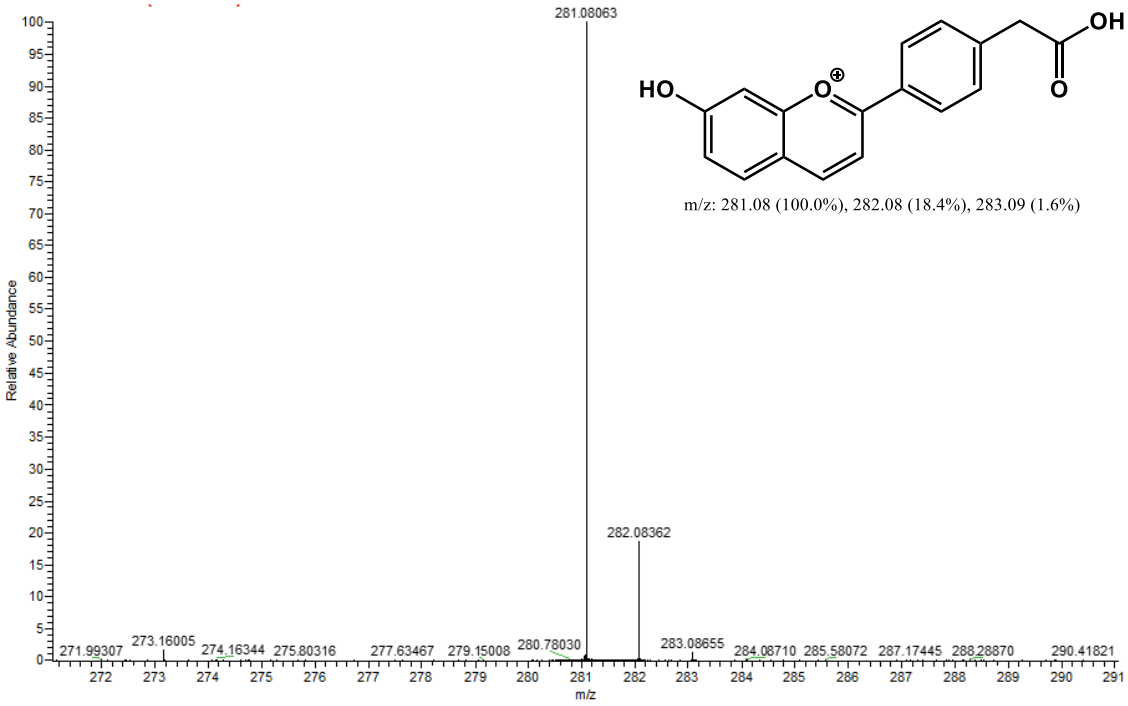

Figure 19 – Mass spectroscopy of 7-hydroxy-4'-methylcarboxyflavylium

1.9. Synthesis of 4'-methylcarboxychalcone (9)

In order to synthesize a flavylium substituted in the position 4 another synthetic approach was needed. The first step was the synthesis of a chalcone containing the carboxylic tail. This was accomplished by the same condensation reaction as reported before for compounds (1), (7) and (8), but this time the reaction was done in alkaline medium.

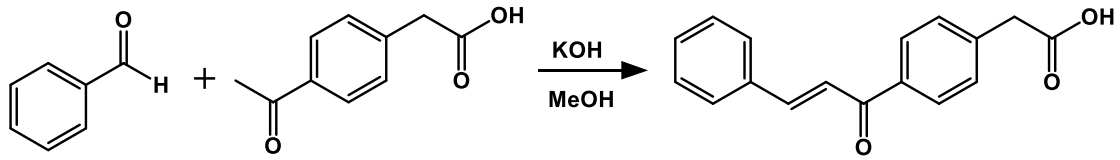

Scheme 20 – Condensation reaction of 4-Acetylphenyl)acetic acid with benzaldehyde

The structure of the as synthesized chalcone was confirmed by NMR and was used in the next step.

1.10. Synthesis of 7-hydroxy-4'-methylcarboxy-4-phenylflavylium (10)

Using the chalcone synthesized in the previous reaction, it was possible to synthesized a flavylium with a carboxylic tail in position 4' and a phenyl ring in position 4. This was accomplished by making another condensation reaction with resorcinol, in acidic conditions.

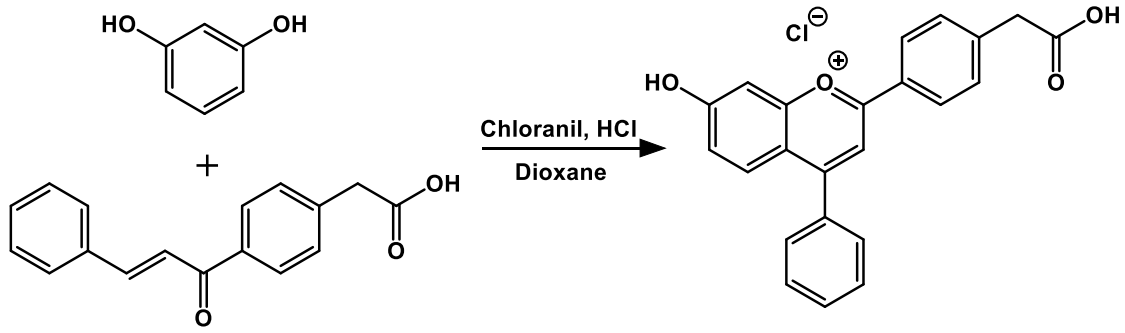

Scheme 21 – Condensation reaction of 4'-methylcarboxychalcone with resorcinol

Chloranil, also known as tetrachloro-1,4-benzoquinone, is a chlorinated quinone that can be used as a mild oxidant and serves as a hydrogen acceptor in aromatization reactions. In this reaction, the presence of chloranil facilitates the ring closure needed to form the flavylium.

In this reaction, HCl was chosen instead of tetrafluorboronic acid used in previous flavylium synthesis. Robinson and Walker[38] reported a similar reaction, in which he used HCl to make a flavylium cation substituted in the position 4. Moreover, in our lab, flavylium synthesized using HCl gas usually have higher reaction yields. This HCl gas is normally generated using the Sulfuric Acid (H_2SO_4) method, in which an aqueous solution of HCl is added drop-wise to a flask containing an aqueous solution of H_2SO_4, when the two solutions mix the HCl solubility in water is decreased and HCl gas is released.

This way of generating HCl gas can be as efficient as 90%, however it requires the use of a complex apparatus, the need for additional security precautions, and produce more waste, mainly H_2SO_4. For these reasons, it was used a commercial solution of HCl in dioxane. This was mainly a test but actually worked and the desired flavylium was obtained with a reaction yield of 33%. The compound structure was confirmed by NMR, elemental analysis and mass spectroscopy (ESI/MS). This flavylium salt was later used to functionalize the CQDs.

Since this is a new flavylium its structure was confirmed by elemental analysis and mass spectroscopy.

Table 3 – Elemental analysis of 7-hydroxy-4′-methylcarboxy-4-phenylflavylium

Formula: $C_{23}H_{17}ClO_4 \cdot (1/2)H_2O$	
Calculated	**Determined**
C: 68.75	C: 68.91
H: 4.51	H: 4.88

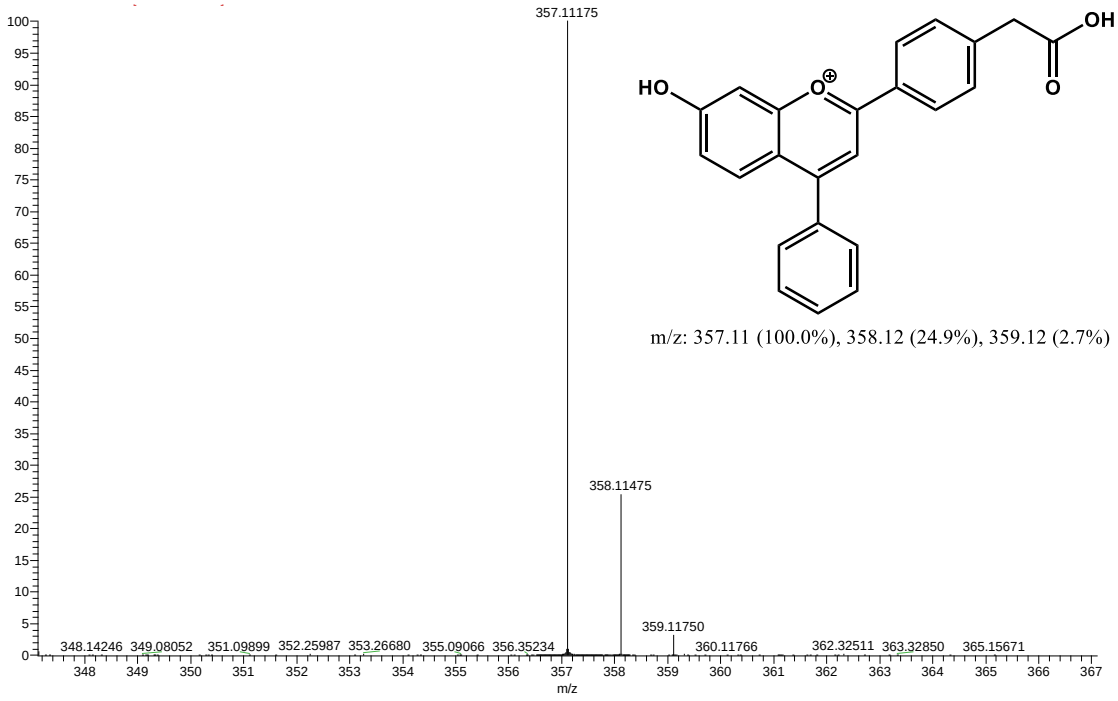

Figure 20 – Mass spectroscopy of 7-hydroxy-4′-methylcarboxy-4-phenylflavylium

1.11. UV-Vis titration of 7-hydroxy-4'-methylcarboxyflavylium (8)

A solution of 7-hydroxy-4'-methylcarboxy-4-phenylflavylium was prepared in water at pH 1 and 1 mL of this solution was transferred to several plastic cuvettes containing 1 mL of NaOH 1 M and 1 mL of phosphate buffer with different pH values. Absorption spectra was obtained for each cuvette immediately after flavylium addition (Figure 21). This technique is known as pH jump and it allows to study the formation and disappearing of intermediate species, like the quinoidal base.

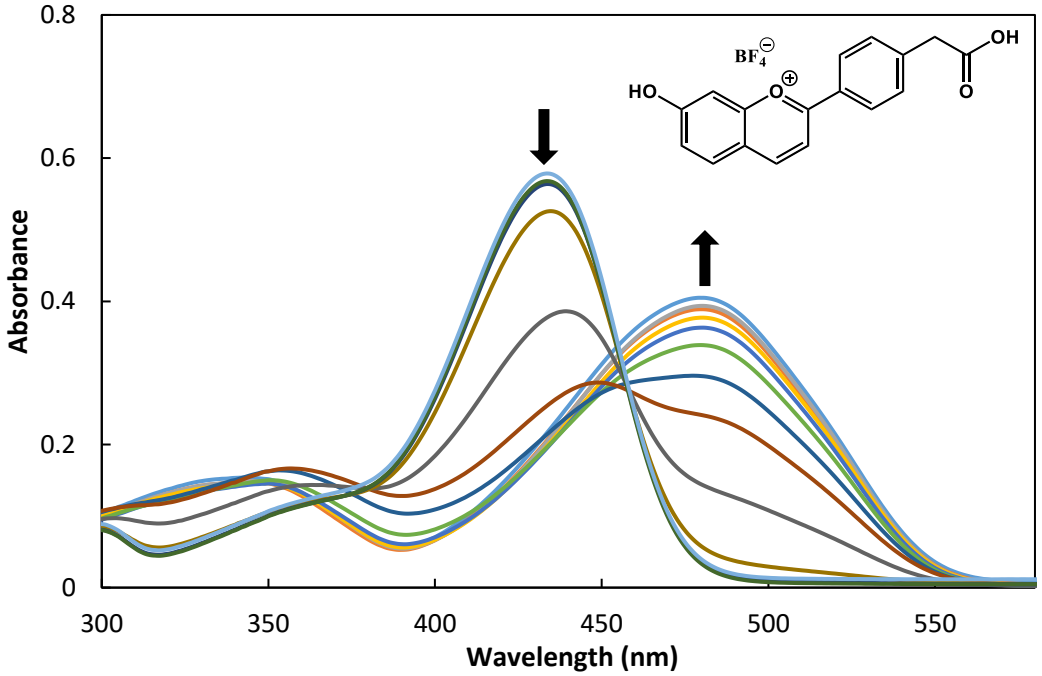

Figure 21 – Absorption spectra of 7-hydroxy-4'-methylcarboxyflavylium (8) after pH jump, as a function of pH, from pH 0.58 to 8.73. Arrows indicate the absorbance variation with increase in pH

After pH jump, two main absorption bands are observed in the visible region, one at 490 nm and other at 440 nm. The band at 440 nm can be attributed to the flavylium cation **AH**$^+$ since it's the major band at low pH and disappear with the increase in pH. Similarly, the band at 490 nm can be attributed to the quinoidal base **A**, the absorption of this band increase with the pH and is red-shifted. It is also observed an isosbestic point at 460 nm (wavelength at which the total absorbance of the sample does not change).

The cuvettes were left in the dark overnight to equilibrate and the absorption spectra was recorded in the next day. (Figure 22) Again, two main absorption bands were observed in the visible region, one at 440 nm and other at 370 nm.

The band at 440 nm has its maximum intensity at pH 0.58 and can be assigned to **AH**$^+$ since it is the only species stable at this low pH. With the increase in pH, this band disappears and gives rise to the band at 370 nm, which was not visible after the pH jump. This indicates that the species responsible for such band must have been formed during the equilibrium, so it can be assigned to the **Ct** species, since this is the most stable species when the system reaches the thermodynamic equilibrium. The absorption in the UV is also compatible with a chalcone species.

At basic pH (> 7), it is also possible to see the formation of a broad absorption band centred at 445 nm (Figure 22, dashed lines), this band is probably due to the formation of **Ct**$^-$, since the increase in this band is accompanied by a decrease in the **Ct** band.

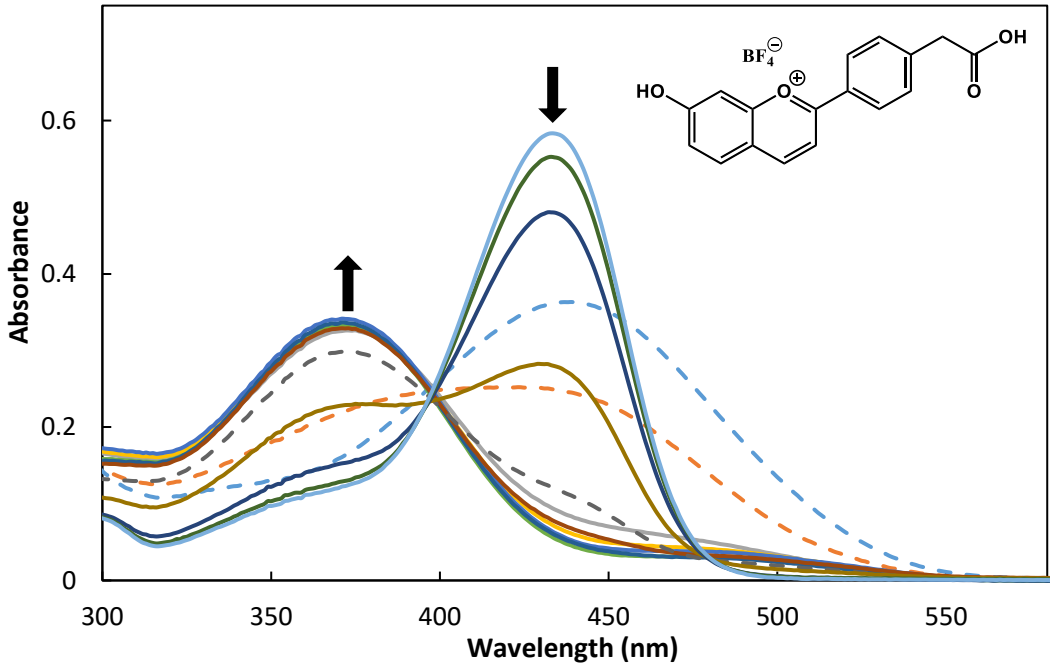

Figure 22 – Absorption spectra of 7-hydroxy-4′-methylcarboxyflavylium (8) after equilibrate in the dark, as a function of pH, from pH 0.58 to 6.6 (solid lines) and from pH 7.04 to 8.73 (dashed lines). Arrows indicate the absorbance variation with increase in pH

The isosbestic point located at 460 nm disappeared and a new isosbestic point appeared at 395 nm.

The various flavylium equilibria in aqueous solution can be described as:

$$A \underset{}{\overset{K_a}{\rightleftharpoons}} AH^+ \overset{K'_a}{\rightleftharpoons} Ct \overset{K_{ct-}}{\rightleftharpoons} Ct^-$$

(eq 1)

Immediately after pH jump, we can consider a simple acid-base equilibrium between the flavylium cation **AH⁺** and the quinoidal base **A**:

$$A \overset{K_a}{\rightleftharpoons} AH^+$$

(eq 2)

The mole fractions of these species, as a function of pH, can be calculated using the following equations:

$$\chi_{AH^+} = \frac{[H^+]}{[H^+] + K_a}$$

(eq 3)

$$\chi_A = \frac{K_a}{[H^+] + K_a}$$

(eq 4)

After equilibrate in the dark, we have to consider the formation of other species and can ignore the presence of **A**:

$$AH^+ \overset{K'_a}{\rightleftharpoons} Ct \overset{K_{ct-}}{\rightleftharpoons} Ct^-$$

(eq 5)

The mole fractions of these species, as a function of pH, can be calculated using the following equations:

$$\boldsymbol{\chi_{AH^+} = \frac{[H^+]^2}{[H^+] + [H^+]K'_a + K'_aK_{ct-}}}$$

(eq 6)

$$\boldsymbol{\chi_{Ct} = \frac{[H^+]K'_a}{[H^+] + [H^+]K'_a + K'_aK_{ct-}}}$$

(eq 7)

$$\boldsymbol{\chi_{Ct^-} = \frac{K'_aK_{ct-}}{[H^+] + [H^+]K'_a + K'_aK_{ct-}}}$$

(eq 8)

The equilibrium constants K_a, K'_a, and K_{ct^-} can be determined by fitting the absorbance at the flavylium absorption maximum (440nm), calculated using (eq 9), with the experimental data. (Figure 23)

$$A = \chi_{AH^+} \times A_{AH^+} + \chi_A \times A_A + \chi_{Ct} \times A_{Ct} + \chi_{Ct^-} \times A_{Ct^-}$$

(eq 9)

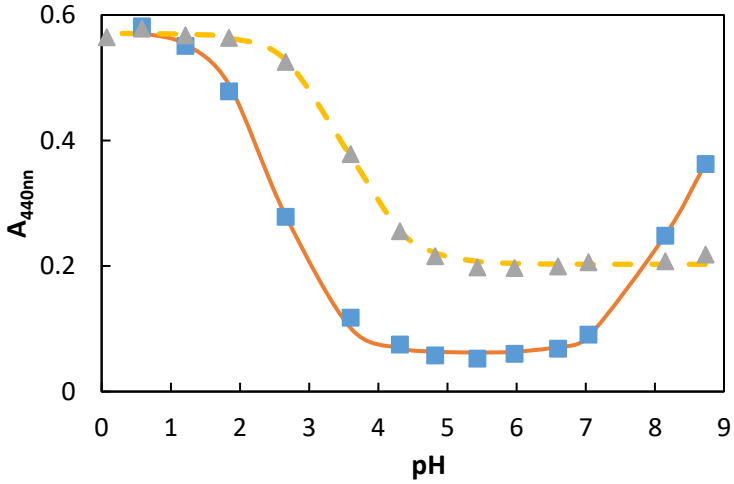

Figure 23 –Variation of absorbance at 440nm: experimental values after pH jump (▲) and after equilibrate in the dark (■); and values calculated using equation 5, after pH jump (dashed line) and after equilibrate in the dark (solid line)

Fitting was achieved for $pK_a = 3.54$ ($K_a = 2.85 \times 10^{-4}$), after pH jump, and for $pK'_a = 2.53$ ($K'_a = 2.96 \times 10^{-3}$) and $pK_{ct^-} = 8.17$ ($K_{ct^-} = 6.80 \times 10^{-9}$), after equilibrate in the dark.

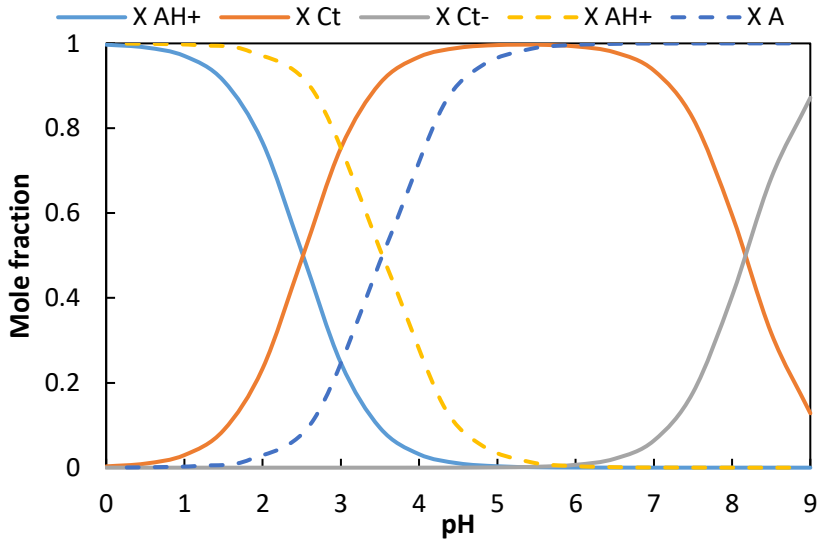

Figure 24 – Mole fraction distribution as a function of pH for the 7-hydroxy-4′-methylcarboxyflavylium compound, after pH jump (dashed lines) and after equilibrate in the dark (solid lines)

1.12. UV-Vis titration of 7-hydroxy-4'-methylcarboxy-4-phenylflavylium (10)

The UV-Vis titration was made using the pH jump technique described in 1.11. The obtained absorption spectra are represented in Figure 25.

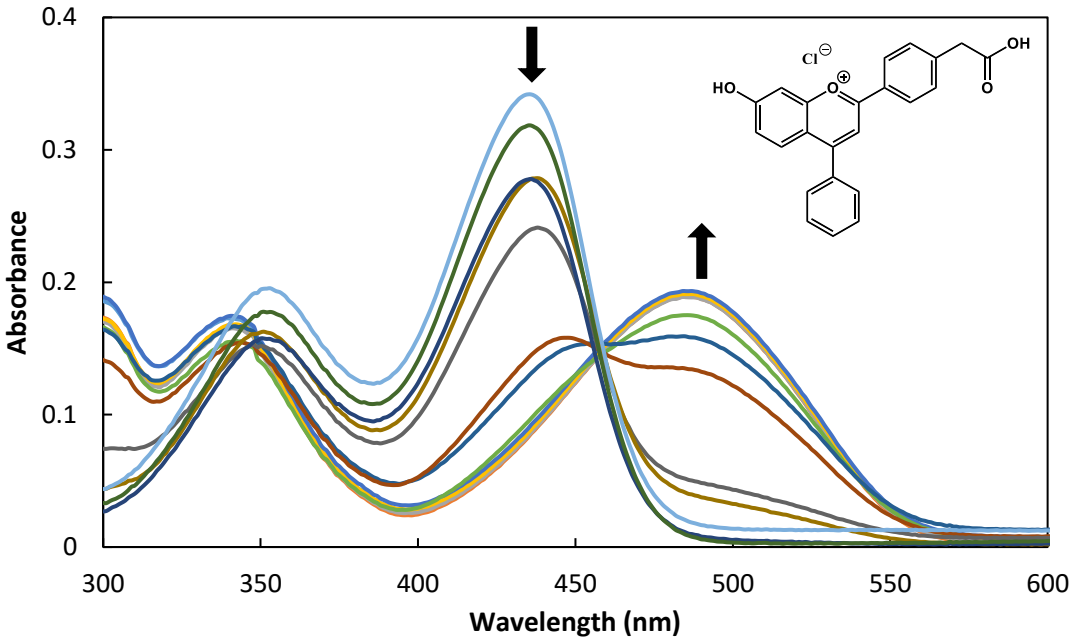

Figure 25 – Absorption spectra of 7-hydroxy-4'-methylcarboxy-4-phenylflavylium after pH jump, as a function of pH, from pH 0.60 to 9.28. Arrows indicate the absorbance variation with increase in pH, for the solid lines

Similar to flavylium (8), after pH jump two main absorption bands are observed in the visible region, one at 490 nm and other at 440 nm. The band at 440 nm can again be attributed to the flavylium cation **AH**$^+$ since it's the major band at low pH and disappear with the increase in pH. Similarly, the band at 490 nm can be attributed to the quinoidal base **A** since the absorption of this band increase with the pH and coincide with the disappearing of **AH**$^+$. Furthermore, is well known that quinoidal bases present a red-shifted absorbance related to the flavylium cation. It is also observed an isosbestic point at 460 nm.

The cuvettes were left in the dark overnight to equilibrate and the absorption spectra was recorded in the next day (Figure 26). Again, two main absorption bands were observed in the visible region, one at 490 nm and other at 400 nm. In the pH range 0.60 – 8.34 there is no significant change in the absorption spectra after the system reached equilibrium. This was expected since it is well known that the addition of a phenyl ring (or a methyl group) in position 4 stabilizes the

AH⁺ species and make the quinoidal base **A** both the kinetic and the thermodynamic product in a wide pH range. Only at pH 8.92 the **A** band started to decrease (Figure 26, dashed lines), presumably because of the formation of **Ct**, however, no absorption band of this species were detected.

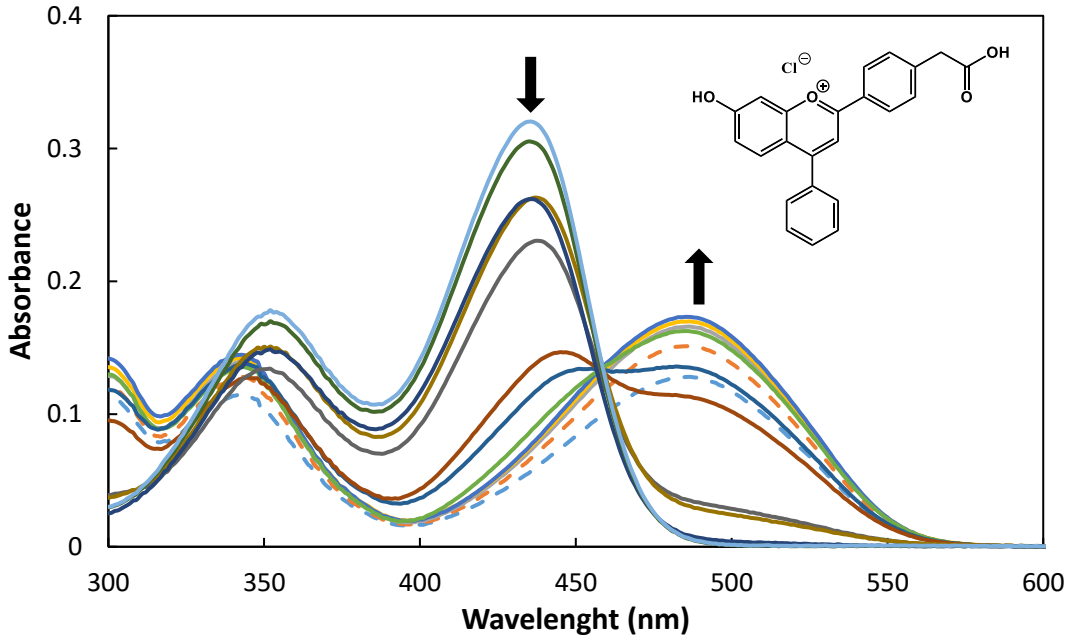

Figure 26 – Absorption spectra of 7-hydroxy-4′-methylcarboxy-4-phenylflavylium (8) after equilibrate in the dark, as a function of pH, from pH 0.60 to 8.34 (solid lines) and from pH 8.92 to 9.28 (dashed lines). Arrows indicate the absorbance variation with increase in pH, for the solid lines

Mole fractions were calculated as described in 1.11.

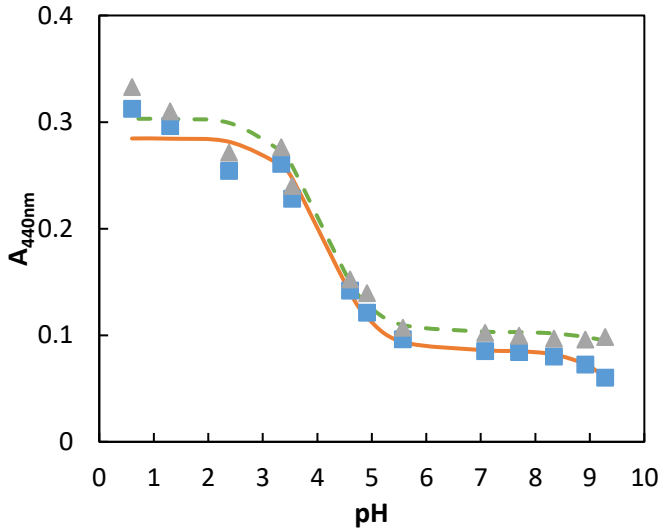

Figure 27 – Variation of absorbance at 440nm: experimental values after pH jump (▲) and after equilibrate in the dark (■); and values calculated using (eq 5), after pH jump (dashed line) and after equilibrate in the dark (solid line)

Fitting was achieved for $pK_a = 4.03$ ($K_a = 9.26 \times 10^{-5}$), after pH jump, and for $pK_a = 4.17$ ($K_a = 6.69 \times 10^{-5}$) and $pK'_a = 9.66$ ($K'_a = 2.18 \times 10^{-10}$), after equilibrate in the dark.

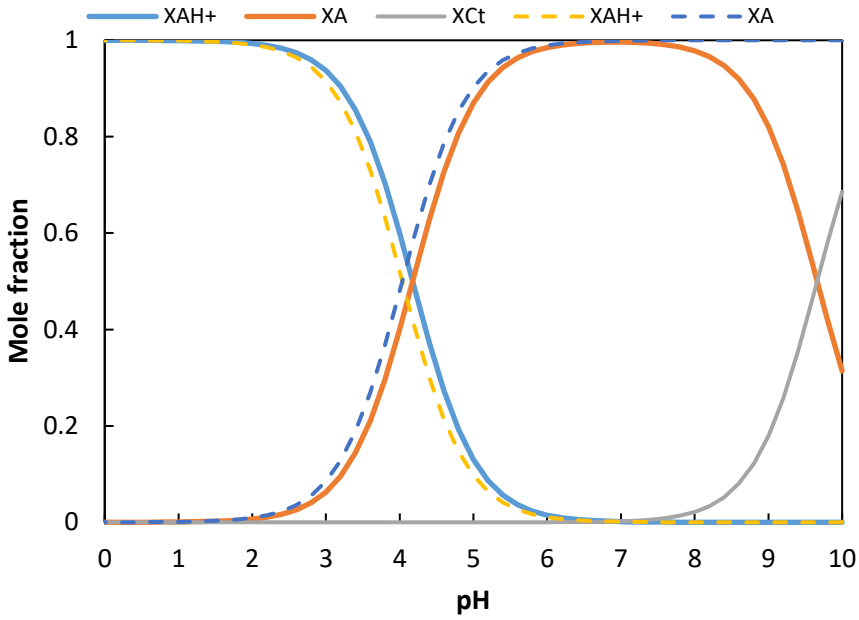

Figure 28 – Mole fraction distribution as a function of pH for the 7-hydroxy-4′-methylcarboxy-4-phenylflavylium compound, after pH jump (dashed lines) and after equilibrate in the dark (solid lines)

1.13. Fluorescence of 7-hydroxy-4'-methylcarboxy-4-phenylflavylium (10)

Steady state fluorescence measurements were performed in order to fully characterize the optical proprieties of 7-hydroxy-4'-methylcarboxy-4-phenylflavylium, the same solutions used in the UV-Vis titration were used. Each solution was transferred to a quartz fluorescence cell before spectra acquisition.

In order to compare the emission of **AH⁺** and **A**, the fluorescence emission spectra were recorded exciting at the isosbestic point, 460 nm. (Figure 29)

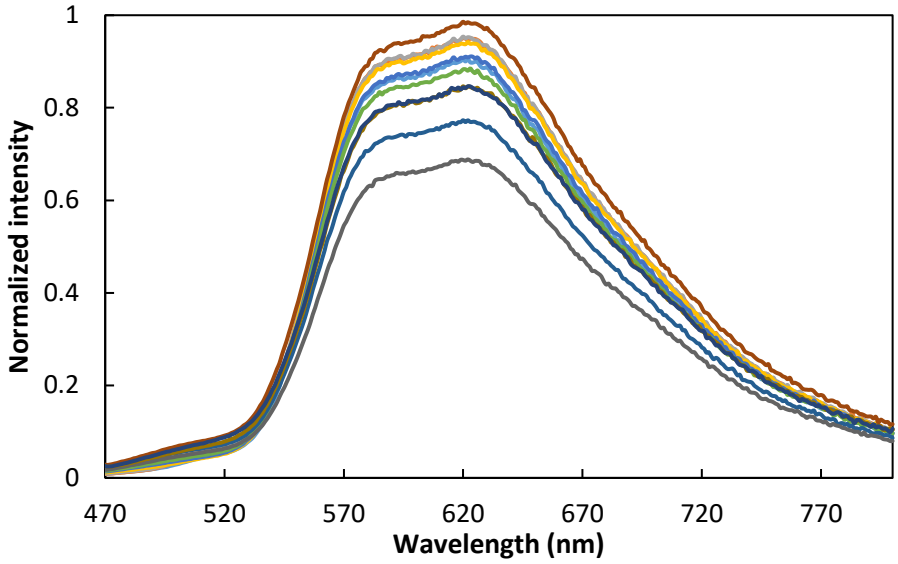

Figure 29 – Fluorescence emission spectra at the excitation wavelength 460 nm (isosbestic point) as a function of pH, from 0.60 to 9.28

Even at low pH values (0.60), there is only a major broad emission band centred around 600 nm. At 480 nm, there is a slight emission band that decreases with the increase in pH, indicating that this band might originate from the **AH⁺** species. That means the broad emission band at 600 nm must be the emission from the base **A**, which makes sense since it is well known that in phenols the fluorescence emission from the basic species is red-shifted in comparison with the emission from the acidic one.

However, as determined before by UV-Vis titration, at low pH there is only **AH⁺** present in solution, so, the emission observed from the base, at low pH, must arise from excited state proton transfer (ESPT), from **AH⁺** to **A**. This was confirmed by the florescence excitation spectra collected monitoring the emission at 600 nm. (Figure 30)

These excitation spectra almost coincide with the absorption spectra (Figure 26), indicating that the base emission arises from ESPT, at low pH values, and as the pH increases it originate from direct base excitation.

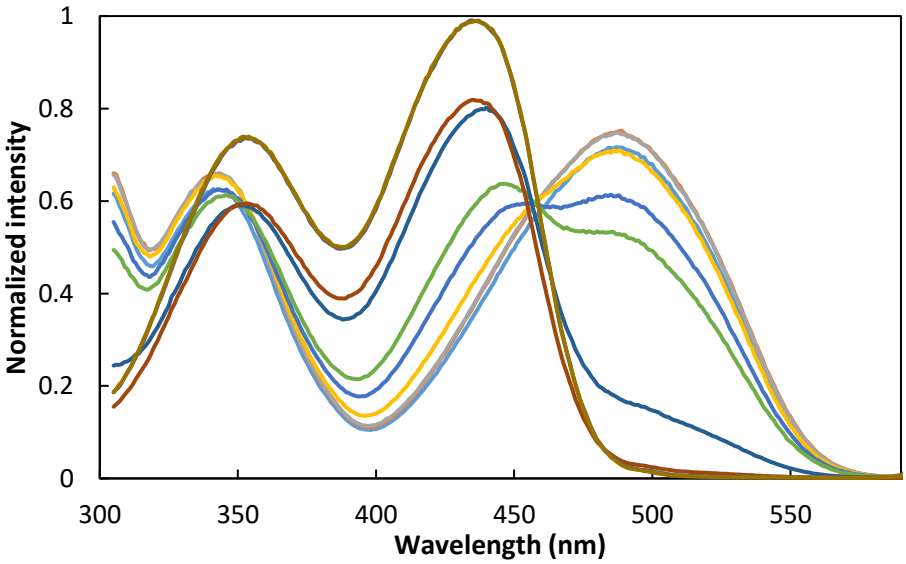

Figure 30 – Fluorescence excitation spectra collecting at 600nm (**A** emission) as a function of pH, from 0.60 to 9.28

In order to observe emission from $\mathbf{AH^+}$ species, fluorescence spectra were recorded exciting only the flavylium cation, at 430 nm. (Figure 31)

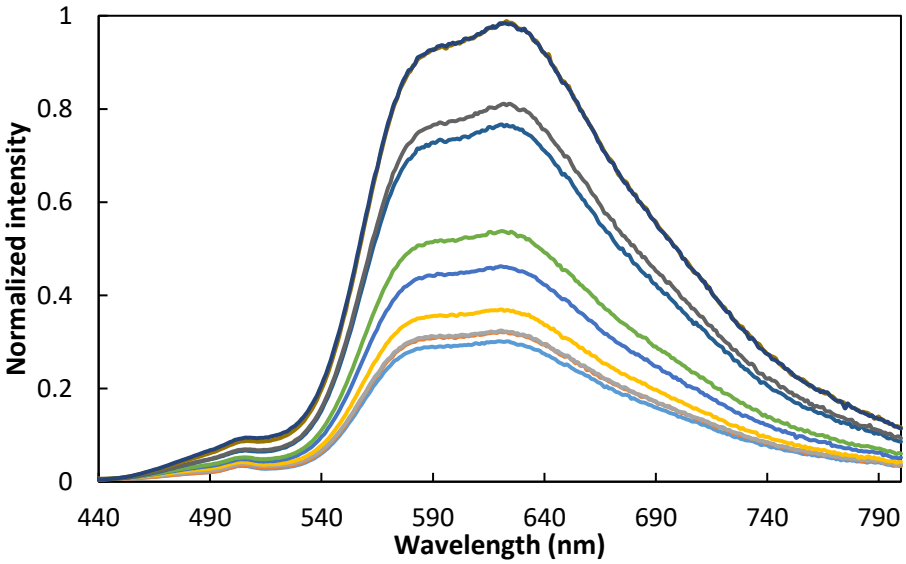

Figure 31 – Fluorescence emission spectra at the excitation wavelength 430 nm ($\mathbf{AH^+}$) as a function of pH, from 0.60 to 9.28

Even exciting at 430 nm, the major emission band continues to be the emission from the base species, indicating a very efficient ESPT. There is a small band around 490-510 nm that can be the emission of flavylium cation.

4

Flavylium-Functionalized CQDs

In this chapter, it is discussed the functionalization of CQDs with two different novel flavylium salts. The functionalization was made by covalently attaching flavylium salts at the CQDs surface. This was accomplished using EDC as a crosslinking agent between the flavylium carboxyl tail and primary amines present at CQDs surface.

The CQDs functionalized with 7-hydroxy-4'-methylcarboxy-4-phenylflavylium were then submitted to the same optical characterization as discussed before for the free CQDs and flavylium, in order to understand how the attachment of flavylium at the CQD surface influence these optical proprieties.

1.1. Functionalization of CQDs with flavylium salts

The QCDs functionalization were performed as described before, using EDC and NHS to covalently bond the flavylium carboxyl tail to primary amines at CQD surface, forming an amide.

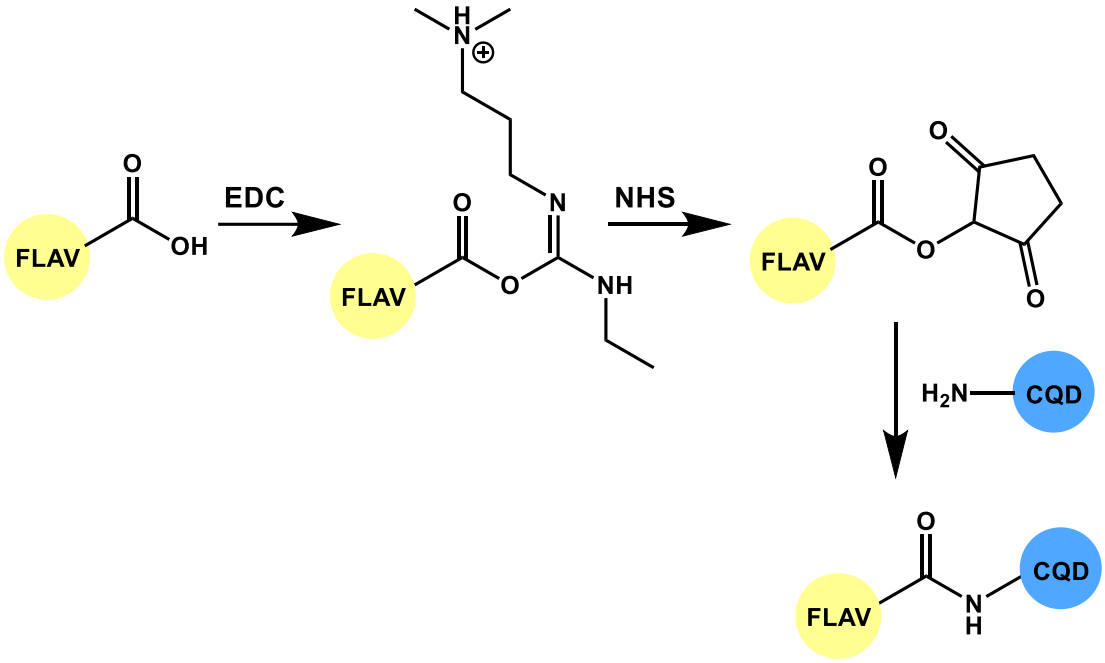

Scheme 22 – General scheme for crosslinking reaction using EDC and NHS

After reaction with EDC and NHS, in ethanol, the functionalized CQDs were dialyzed against ethanol for 48 h (molecular weight cut off was 1 kDa). Solutions were stored at 4 ^{o}C before characterization.

1.2. CQDs functionalized with 7-hydroxy-4'-methylcarboxy-4-phenylflavylium

First, the flavylium functionalized CQDs were characterized by UV-Vis titration. This titration was made using the pH jump technique described before. The obtained absorption spectra are represented in Figure 32.

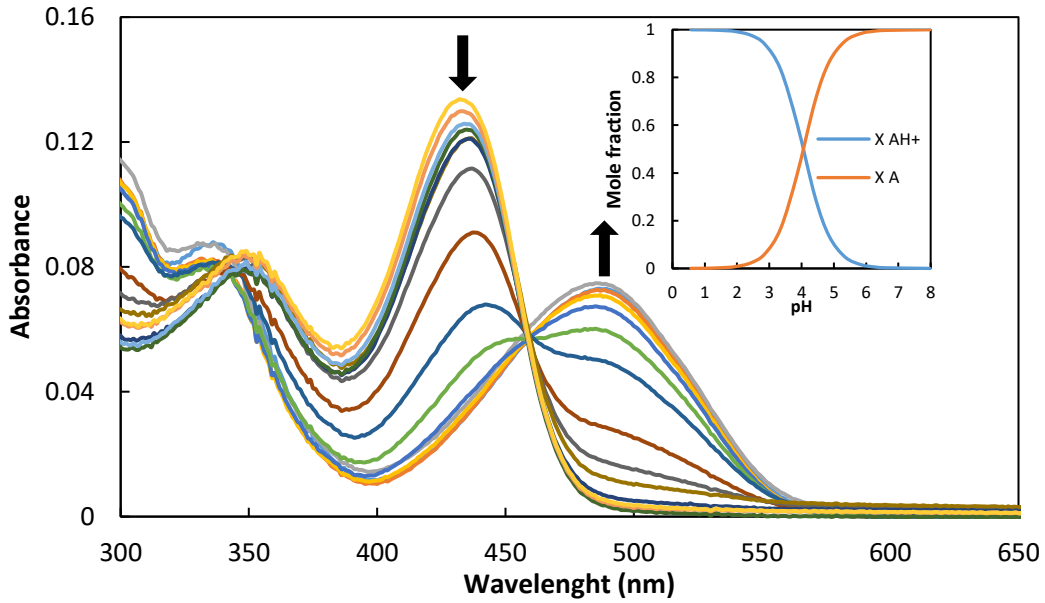

Figure 32 – Absorption spectra of CQDs functionalized with 7-hydroxy-4'-methylcarboxy-4-phenylflavylium after equilibrate in the dark, as a function of pH, from pH 0.57 to 7.98. Arrows indicate the absorbance variation with increase in pH. Inset: Mole fraction of **AH**$^+$ and **A**

Similar to the UV-Vis titration of the free flavylium, two main absorption bands are observed in the visible region, one at 490 nm and other at 440 nm. The band at 440 nm can again be attributed to the flavylium cation **AH**$^+$ and the band at 490 nm can be attributed to the quinoidal base **A**. It is also observed an isosbestic point at 460 nm.

Fitting was achieved for pKa = 4.05 (Ka = 8.93 × 10^{-5}), which represent a shift in pKa of only 0.02, compared to free flavylium. Therefore, is possible to conclude that the attachment of CQDs did not disturbed the equilibrium between **AH**$^+$ and **A**.

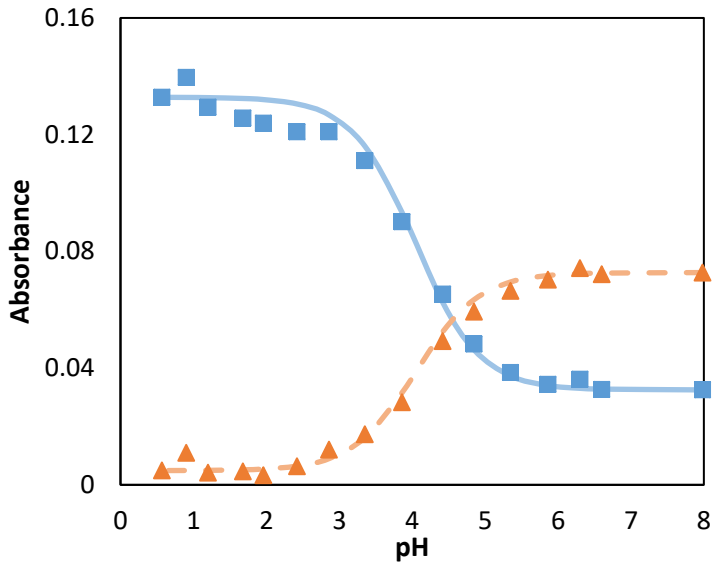

Figure 33 – Variation of absorbance: experimental values at 490 nm (▲) and at 435 nm (■); and values calculated using (eq 9), at 490 nm (dashed line) and at 435 nm (solid line)

Steady-state fluorescence measurements were also made in order to study how CQDs functionalization influenced the photoluminescence properties.

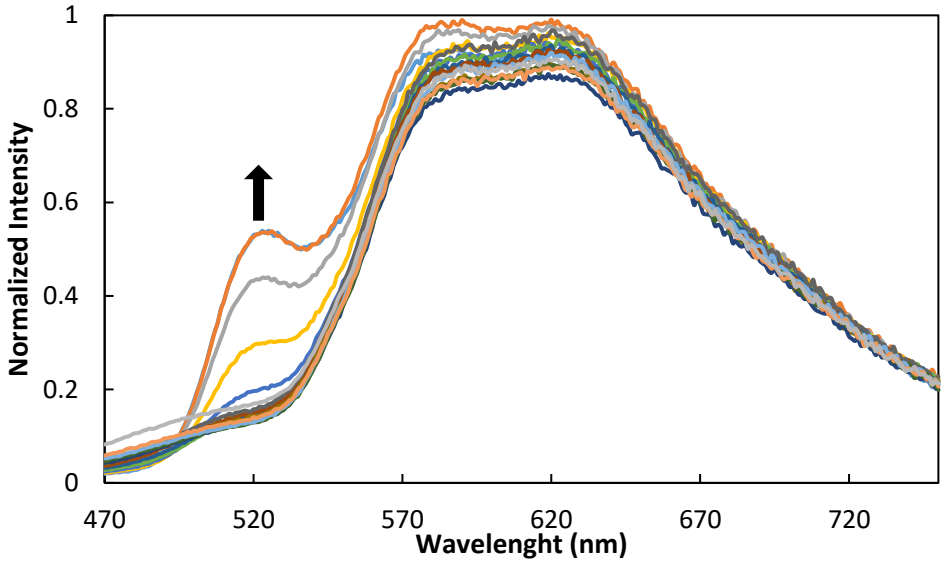

Figure 34 – Fluorescence emission spectra at the excitation wavelength 460 nm (isosbestic point) as a function of pH, from 0.57 to 7.98

Exciting at the isosbestic point (460 nm), it is possible to observed the broad emission band of the quinoidal base at 600 nm. It is also possible to observe an emission band centred at 520 nm, this band appears at pH 4.85 and reaches its maximum intensity around pH 6.60. Fluorescence studies of the free flavylium did not shown any emission band in this region, also, it is thought that the flavylium emission is located around 480 nm.

Additional fluorescence emission spectra were recorded exciting at 430 nm (**AH**$^+$) and at 490 nm (**A**), in order to investigate the origin of the emission band at 520 nm. (Figure 35)

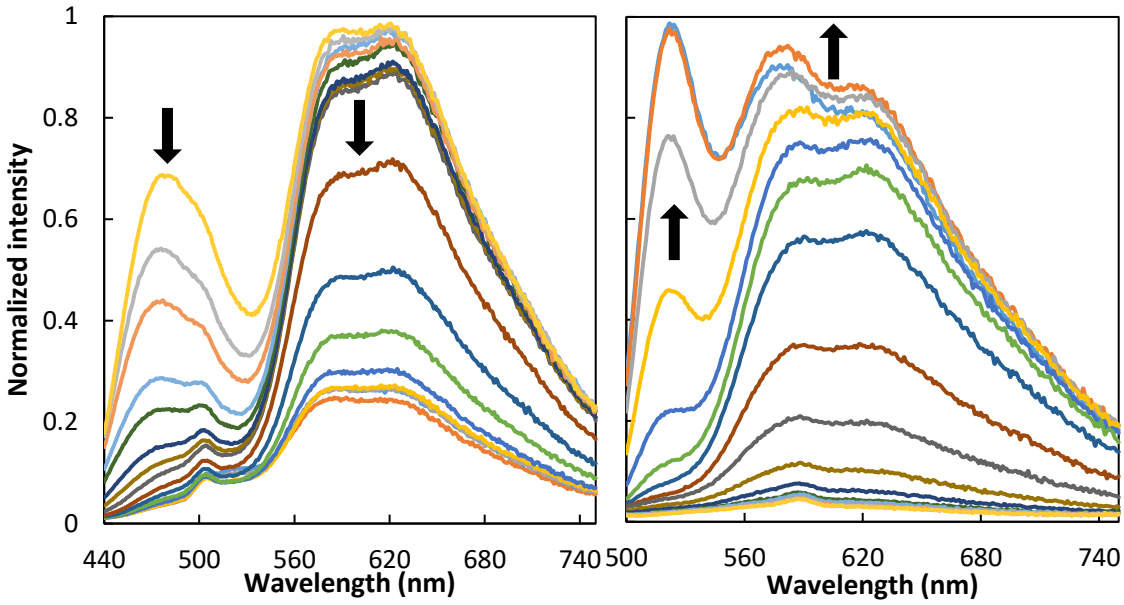

Figure 35 – Fluorescence emission spectra at the excitation wavelength 430 nm (left) and 490 nm (right) as a function of pH, from 0.57 to 7.98

Exciting at 430 nm, is possible to observe a broad emission band centred at 480 nm, before attachment of CQDs this band was not visible (Figure 31). The intensity decreases with increase in pH, indicating that this emission may originate from the **AH**$^+$ species. However, even at low pH, the emission band from the base is still visible at 600 nm, meaning that the ESPT is still significant in these conditions.

Exciting at 490 nm is possible to observe only base emission (pH < 5) but as the pH increases the emission band at 520 nm becomes more intense and at pH 6.6 becomes the dominant band. The increase in pH also led to an increase in base emission, as expected, since more base exists at higher pH. However, this raises

the question, if flavylium cation is forming the quinoidal base, then what is forming the species responsible for this emission at 520 nm?

To try to answer that question, it was made a fluorescence excitation spectra collecting at 520 nm and at 600nm. (Figure 36)

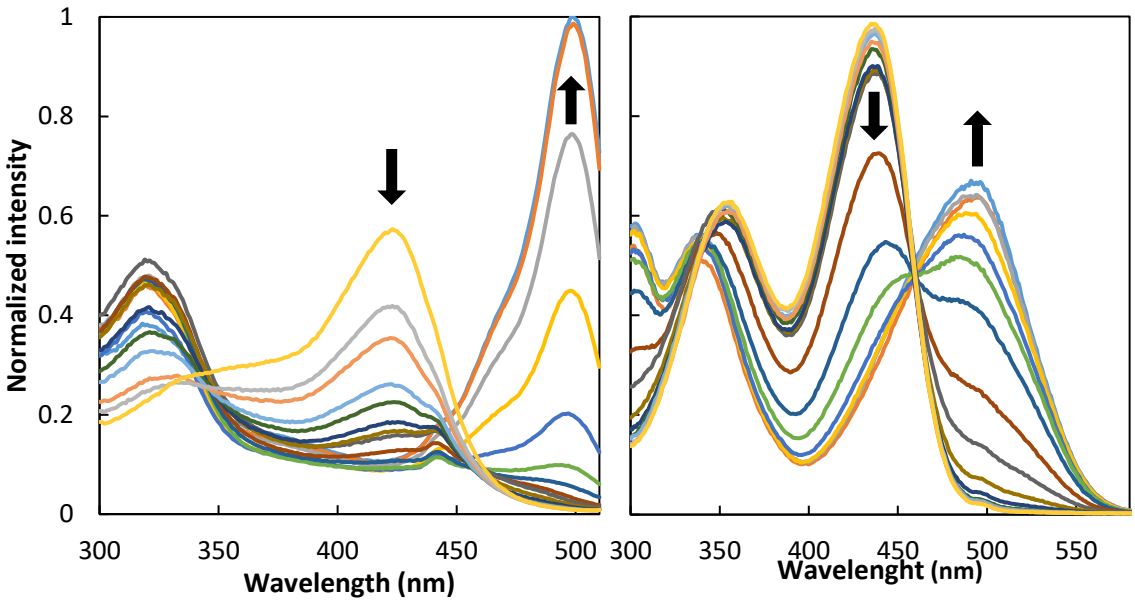

Figure 36 – Fluorescence excitation spectra collecting at 520 nm (left) and at 600 nm (right) as a function of pH, from 0.57 to 7.98. Arrows indicate the intensity variation with increase in pH.

The excitation spectra collecting at 520 nm, revealed two major excitation bands, one centred at 425 nm and other at 500 nm. The excitation band at 425 nm have its maximum intensity at pH 0.57 and then start to decrease intensity as the pH raises. Contrary, the band at 500 nm have its minimum at pH 0.57 and becomes more intense as the pH increases, reaching its maximum at pH 6.6. This behaviour is similar to that observed for the acid-base equilibrium between $\mathbf{AH^+}$ and **A**. This result indicates that this band originates from both the $\mathbf{AH^+}$ and the **A** species, however, the mechanism of PL is still unclear.

The excitation spectra collecting at 600 nm is identical to the absorbance spectra (Figure 32), confirming that the base emission originate from ESPT from $\mathbf{AH^+}$ to **A**, at low pH value, and from direct base excitation at higher pH. This is same behaviour observed for the free flavylium. (Figure 30)

5

Conclusions

In the case of 7-hydroxy-4-phenylflavylium, two species are observed, the acid (**AH**$^+$) and its conjugate base (**A**) resulting from deprotonation of the phenol group with a pKa=4.03 as determined by UV-Vis absorption spectroscopy. Fluorescence studies of the free flavylium cation in aqueous solution allowed us to measure the **AH**$^+$ (490 nm) and the **A** emission (600 nm). When excited at the isosbestic point, only the **A** emission is observed even at very low pH values. At this pH, the excitation spectra collected at 600 nm matches the flavylium absorption spectrum, indicating that the observed emission arises from excited state proton transfer (ESPT) of **AH**$^+$.

When conjugated with CQDs, there is no significant difference in the absorbance spectra, however, the **AH**$^+$ emission appears at low pH range (< 2). This points out to a decrease in the ESPT efficiency, indicating a different environment at the QCDs surfaces. The CQDs broad emission band (450 nm) was supressed after functionalization with flavylium cations, which may indicate resonance energy transfer from CQDs to the flavylium species.

The fluorescence emission spectra also exhibited a new band at 520 nm. The origin of this band is not yet fully understood and more experimental and theoretical work is needed.

6

Experimental Part

1.1. Materials

All glassware used to air sensitive experiments were oven-dried at least 2 hours before use and left to cool in a desiccator.

Moisture-sensitive reactions were carried out under nitrogen atmosphere, dried in a $CaCl_2$ column.

Molecular sieves (4 A, 4-8 mesh) purchased from Aldrich were activated by heating in an oven at 400°C for 1 day.

Reagents

All reagents were of analytical grade and were used as purchased from the manufactures, without further purification.

Solvents

Prior to use, THF was dried over activated molecular sieves (20%) during 2 days, under nitrogen atmosphere.

All other solvents were used as delivered.

1.2. Equipment

NMR Spectroscopy: NMR spectra were recorded on a Brucker AMX400 operating at 400,13 MHz (^{1}H) and at 100 MHz (^{13}C). Chemical shifts (δ) are reported in parts per million (ppm). ^{1}H shifts are referenced to chloroform-d (δ = 7.26), acetonitrile-d (δ=1.94) or water-d2 (δ = 4.79). ^{13}C shifts are referenced to chloroform-d (δ = 77.16), or acetonitrile-d (δ = 1.32). Splitting patterns were represented as follow: s for singlet; d for doublet; t for triplet; q for quartet and m for multiplet.

Absorbance spectroscopy: Absorbance measurements were made in a Varian-Cary 100 Bio, operating at room temperature (21 ^{o}C).

Fluorescence spectroscopy: Fluorescence measurements were made in a SPEX Fluorolog F111 with right angle geometry. Temperature was kept at 21 ^{o}C. Quartz cells with an optical path of 1 cm were used.

Mass spectroscopy (ESI-MS): The utilized instrument was a LTQ Orbitrap XLTM mass spectrometer (Thermo Fischer Scientific) controlled by LTQ Tune Plus 2.5.5 and Xcalibur 2.1.0. The capillary voltage of the electrospray ionization (ESI) was set to 3100 V. The capillary temperature was 275^{o}C. The sheath gas flow rate (nitrogen) was set to 5 (arbitrary unit as provided by the software settings). The capillary voltage was 33 V and the tube lens voltage 100 V.

Balance: Weight measurements were made in a Sartorius Research R200D balance with 5 decimal plates and ±0,01 mg precision.

Elemental analysis: Mass fractions of C and H were determined in a Thermo Finnigan Flash A serie 1112.

TEM: Images acquired in a Hitachi 8100 with Thermo Noran light elements EDS detector and digital image acquisition.

1.3. Generals Procedures

a. Synthesis of 4'-metoxyflavylium (1)

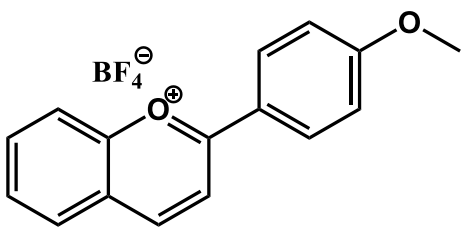

2-hidroxybenzaldehyde (20 mmol) and 4-metoxyacetophenone (20mmol) were dissolved in acetic acid (25 mL) and HBF4 (5 mL, 48-50%) while stirring. Acetic anhydride (25 mL) was added dropwise to maintain the temperature of the reaction mixture at 60 °C until no more exothermic reaction was observed. After stirring at room temperature for about 12 h and the addition of ethyl acetate (50 mL), the precipitate was filtered off and recrystallized from glacial acetic acid yielding (1) as a bright orange powder (2.36625 g, 7.3 mmol, 33.8%).

^{1}H NMR (400 MHz, D_2O/DCl) δ 8.74 (d, J = 9.0 Hz, 1H), 8.01 (d, J = 9.1 Hz, 1H), 7.92 (d, J = 8.9 Hz, 2H), 7.84 – 7.73 (m, 2H), 7.70 (d, J = 8.6 Hz, 1H), 7.47 (t, J = 7.7 Hz, 1H), 6.66 (d, J = 8.9 Hz, 2H), 3.49 (s, 3H).

b. Synthesis of 4-benzotriazol-4'-metoxyflavylium (2)

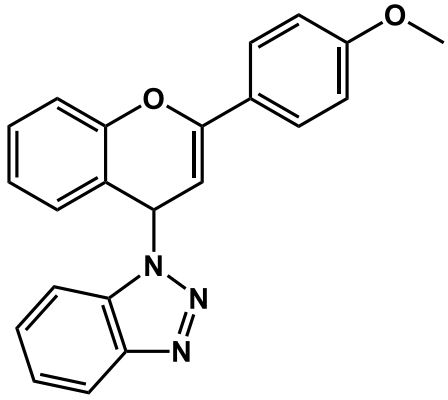

To a solution of benzotriazole (1.19g, 10 mmol) in dry THF (50 mL) was added NaH (0.40g of 60% in mineral oil, 10 mmol). The reaction mixture was stirred at room temperature for 20 min before adding (1) (10 mmol). The reaction mixture was left stirring for 20 min before the precipitated inorganic by-product was filtered off. After evaporation of the solvent, the crude product was purified by recrystallization from ethanol, and isolated as colourless microcrystals. (1.3131 g, mmol, 84.7 %).

^{1}H NMR (400 MHz, $CDCl_3$) δ 8.02 (d, J = 7.8 Hz, 1H), 7.72 (d, J = 8.9 Hz, 2H), 7.38 – 7.15 (m, 9H), 7.07 – 7.01 (m, 1H), 6.95 (t, J = 7.1 Hz, 2H), 5.71 (d, J = 4.5 Hz, 1H), 3.86 (d, J = 8.2 Hz, 3H).

c. Synthesis of 4-ethylacetate-4'-metoxyflavylium (3)

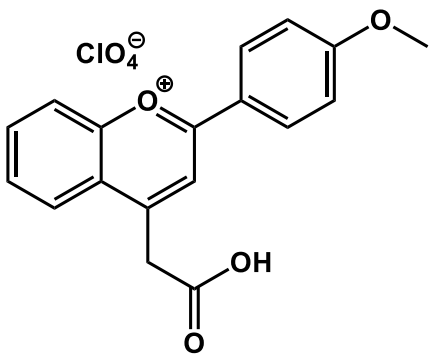

To a solution of (2) (0.625 mmol) in dry THF (25 mL) at -95 °C, was added n-BuLi (0.61 mL, 0.625 mmol, 1.6M in hexane). The solution was stirred at -95 °C for 30 min, before adding the ethylbromoacetate (0.625 mmol) as a solution in dry THF (7.5 mL). The reaction mixture was stirred overnight and allowed to warm up to room temperature, before being quenched with saturated aqueous NH_4Cl solution (30 mL), and extracted with diethyl ether (2 × 30 mL). The combined organic extracts were washed with brine and then dried with $MgSO_4$. The solvent was removed in vacuum and the resulting oil dissolved in acetic acid (20 mL) and $HClO_4$ (0.4 mL, 70%). The precipitate formed after the addition of water (50 mL) was collected by filtration and recrystallized from glacial acetic acid.

Resulting compound was not stable in aqueous solution.

d. Synthesis of 4-(bromomethyl)acetophenone (4)

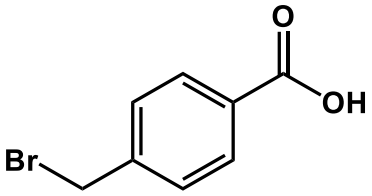

4-Methylacetophenone (5.0 mL, 37.25 mmol, 1.0 eq) was dissolved in acetonitrile (40 mL) under nitrogen. NBS (7.3 g, 41.0 mmol, 1.1 eq) and AIBN (0.615 g, 3.75 mmol, 0.1eq) were added and the reaction mixture was stirred for 1.5 h at 90°C to give a yellow solution. The solvent was removed in vacuum, the residue taken up in toluene (50 mL) and the solution filtrated. After removal of the solvent, purification by silica gel column chromatography (n-pentane / EtOAc 10:1 → 5:1) yielded (4) as a white solid (15.1 g, 70.7 mmol, 95 %).

^{1}H NMR (400 MHz, $CDCl_3$) δ 7.96 (d, J = 8.3 Hz, 1H), 7.51 (d, J = 8.3 Hz, 1H), 4.53 (s, 1H).

e. Synthesis of (4-Acetylphenyl)acetonitrile (5)

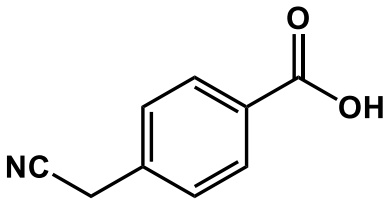

(4) (4.5195 g, 21.21 mmol, 1.0 eq) was dissolved in dioxane (40 mL) and KCN (1.9536 g, 30.0 mmol, 1.4 eq) in water (40 mL) was added. The solution was heated to reflux for 2 h (90°C) while stirring; after cooling to room temperature the deep red solution was extracted with EtOAc (3 x 60 mL), the combined organic phases were washed with brine (2 x 60 mL) and dried with $MgSO_4$. Solvents were evaporated and a red solid was obtained. Purification by silica gel column chromatography (n-pentane / EtOAc 2:1) gave (5) as a light red solid (1.8436 g, 11.5 mmol, 53.9%).

^{1}H NMR (400 MHz, $CDCl_3$) δ 7.99 (d, J = 8.1 Hz, 1H), 7.46 (d, J = 8.1 Hz, 1H), 3.84 (s, 1H).

^{13}C NMR (101 MHz, $CDCl_3$) δ 197.28 (s), 136.90 (s), 134.98 (s), 129.15 (s), 128.21 (s), 117.06 (s), 26.65 (s), 23.66 (s).

f. Synthesis of (4-Acetylphenyl)acetic acid (6)

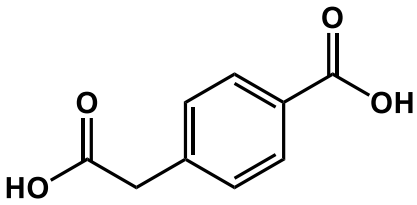

(5) (1.8436 g, 11.5 mmol) was suspended in a mixture of water (40 mL), glacial acetic acid (40 mL) and sulfuric acid (40 mL) and heated to reflux for 90 min (100 °C). To the clear solution was added NaOH (25 g) and water until a total volume of 200 mL was reached. After the NaOH was fully dissolved, the solution was allowed to cool to room temperature and extracted with EtOAc (3 x 80 mL). The combined organic phases were washed with brine (100 mL) and dried with $MgSO_4$. Removal of the solvent yielded (6) as a colourless solid (1.7423 g, 9.78 mmol, 84.4 %).

^{1}H NMR (400 MHz, $CDCl_3$) δ 7.95 (d, J = 8.3 Hz, 2H), 7.41 (d, J = 8.2 Hz, 2H), 3.74 (s, 2H).

^{13}C NMR (101 MHz, CDCl3) δ 197.82 (s), 176.28 (s), 138.58 (s), 136.22 (s), 129.70 (s), 128.72 (s), 40.84 (s), 26.61 (s)

g. Synthesis of 4'-methylcarboxyflavylium (7)

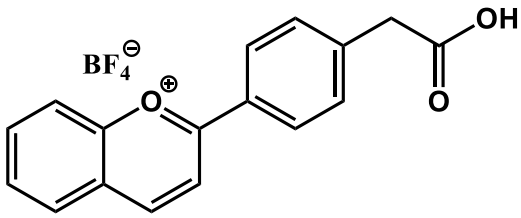

2-hidroxybenzaldehyde (5 mmol) and (6) (5 mmol) were dissolved in acetic acid (5 mL) and HBF4 (1.5 mL, 48-50%) while stirring. Acetic anhydride (5 mL) was added dropwise to maintain the temperature of the reaction mixture at 60 °C until no more exothermic reaction was observed. After stirring at room temperature for about 12 h and the addition of ethyl acetate (20 mL), the precipitate was filtered off and recrystallized from glacial acetic acid yielding (7) as a bright orange powder (1.40738 g, 3.99 mmol, 79.7 %)

^{1}H NMR (400 MHz, CD3CN) δ 9.81 (s, 1H), 9.21 (d, J = 8.5 Hz, 1H), 8.41 (d, J = 8.5 Hz, 2H), 8.36 (d, J = 8.6 Hz, 1H), 8.24 (d, J = 9.0 Hz, 1H), 7.69 (d, J = 8.4 Hz, 2H), 7.63 (d, J = 1.5 Hz, 1H), 7.55 (dd, J = 9.0, 2.2 Hz, 1H), 3.86 (s, J = 12.5 Hz, 2H).

h. Synthesis of 7-hydroxy-4'-methylcarboxyflavylium (8)

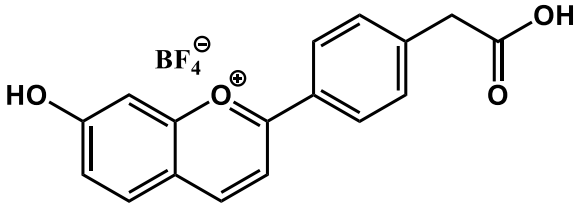

2,4-dihidroxybenzaldehyde (2 mmol) and (6) (2 mmol) were dissolved in acetic acid (5 mL) and HBF4 (1.25 mL, 48-50%) while stirring. Acetic anhydride (5 mL) was added dropwise to maintain the temperature of the reaction mixture at 60 °C until no more exothermic reaction was observed. After stirring at room temperature for about 12 h and the addition of ethyl acetate (20 mL), the precipitate was filtered off and recrystallized from glacial acetic acid yielding (8) as a bright orange powder (0.2750 g, 0.742 mmol, 37.4 %)

^{1}H NMR (400 MHz, CD3CN) δ 9.81 (s, 1H), 9.21 (d, J = 8.5 Hz, 1H), 8.41 (d, J = 8.5 Hz, 2H), 8.36 (d, J = 8.6 Hz, 1H), 8.24 (d, J = 9.0 Hz, 1H), 7.69 (d, J = 8.4 Hz, 2H), 7.63 (d, J = 1.5 Hz, 1H), 7.55 (dd, J = 9.0, 2.2 Hz, 1H), 3.86 (s, J = 12.5 Hz, 2H).

EA: Calculated for $C_{23}H_{17}ClO_4 \bullet H_2O$: C 52.88; H 3.92; determined: C 52.64; H 4.12

ESI/MS: 281.08 (100 %); 282.08 (18.5 %); 283.08 (1.5 %)

i. Synthesis of 4'-methylcarboxychalcone (9)

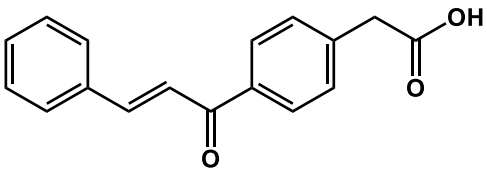

A solution of (6) (2.694 mmol) and benzaldehyde (2.694 mmol) in methanol (10 mL) was cooled to 5–10 °C in an ice bath. The cooled solution was treated with a small portion of pulverized KOH (220 mg). The reaction mixture was stirred for 60 min and then left overnight and was monitored by thin layer chromatography using n-hexane–acetone (5:1) as developing solvent. The resulting dark solution was diluted with ice water and carefully acidified using dilute hydrochloric acid. The chalcone (9), which separated as a yellow solid, were collected by filtration after washing with water and further purified by crystallization from methanol (0.648 g, 2.43 mmol, 90.3 %).

^{1}H NMR (400 MHz, CDCl3) δ 8.02 (d, J = 8.2 Hz, 2H), 7.84 (d, J = 15.7 Hz, 1H), 7.66 (dd, J = 6.3, 2.7 Hz, 2H), 7.54 (d, J = 15.7 Hz, 1H), 7.45 (dd, J = 7.4, 5.6 Hz, 5H), 7.28 (s, 1H), 3.77 (s, 2H), 3.51 (s, 1H), 2.20 (s, 4H).

j. Synthesis of 7-hydroxy-4'-methylcarboxy-4-phenylflavylium (10)

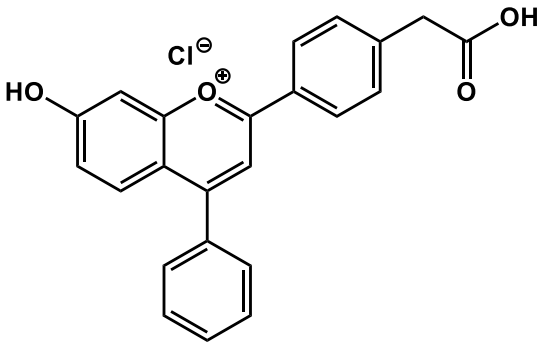

(9) (0.2g, 0.7567 mmol), resorcinol (0.08332 g, 0.7567 mmol) and chloranil (0.186 g, 0.7567 mmol) were dissolved in dioxane (6.25 mL) and a solution of HCl in dioxane was added (3.75 mL, 4M). After stirring at room temperature for about 12 h and the addition of ethyl acetate (50 mL), the precipitate was filtered off and recrystallized from ethanol yielding (10) as a bright orange powder (0.09 g, 0.252 mmol, 33.3%).

^{1}H NMR (400 MHz, CD3CN) δ 8.44 (d, J = 8.4 Hz, 1H), 8.32 (s, 1H), 8.16 (d, J = 9.3 Hz, 1H), 7.88 – 7.72 (m, 3H), 7.68 (d, J = 8.4 Hz, 1H), 7.57 (dd, J = 9.3, 2.2 Hz, 1H), 3.85 (s, 2H), 3.63 (s, 2H).

EA: Calculated for $C_{23}H_{17}ClO_4 \bullet (1/2)H_2O$: C 68.75; H 4.51; determined: C 68.91; H 4.88

ESI/MS: 357.11 (100 %); 358.12 (24.9 %); 359.12 (2.7 %)

7

Appendices

^{1}H NMR spectra of 4′-metoxyflavylium (1)

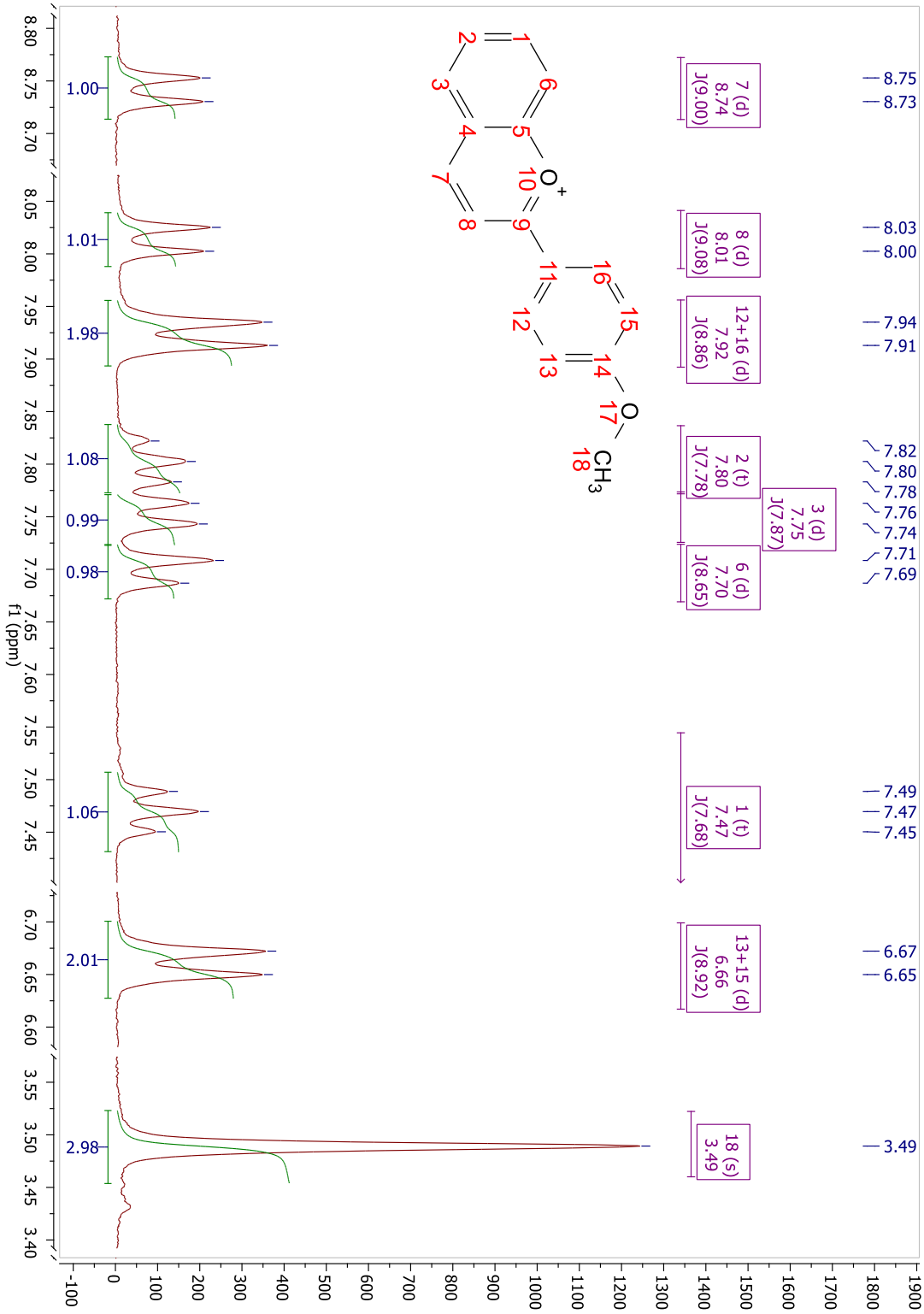

^{1}H NMR spectra of 4-benzotriazol-4′-metoxyflavylium (2)

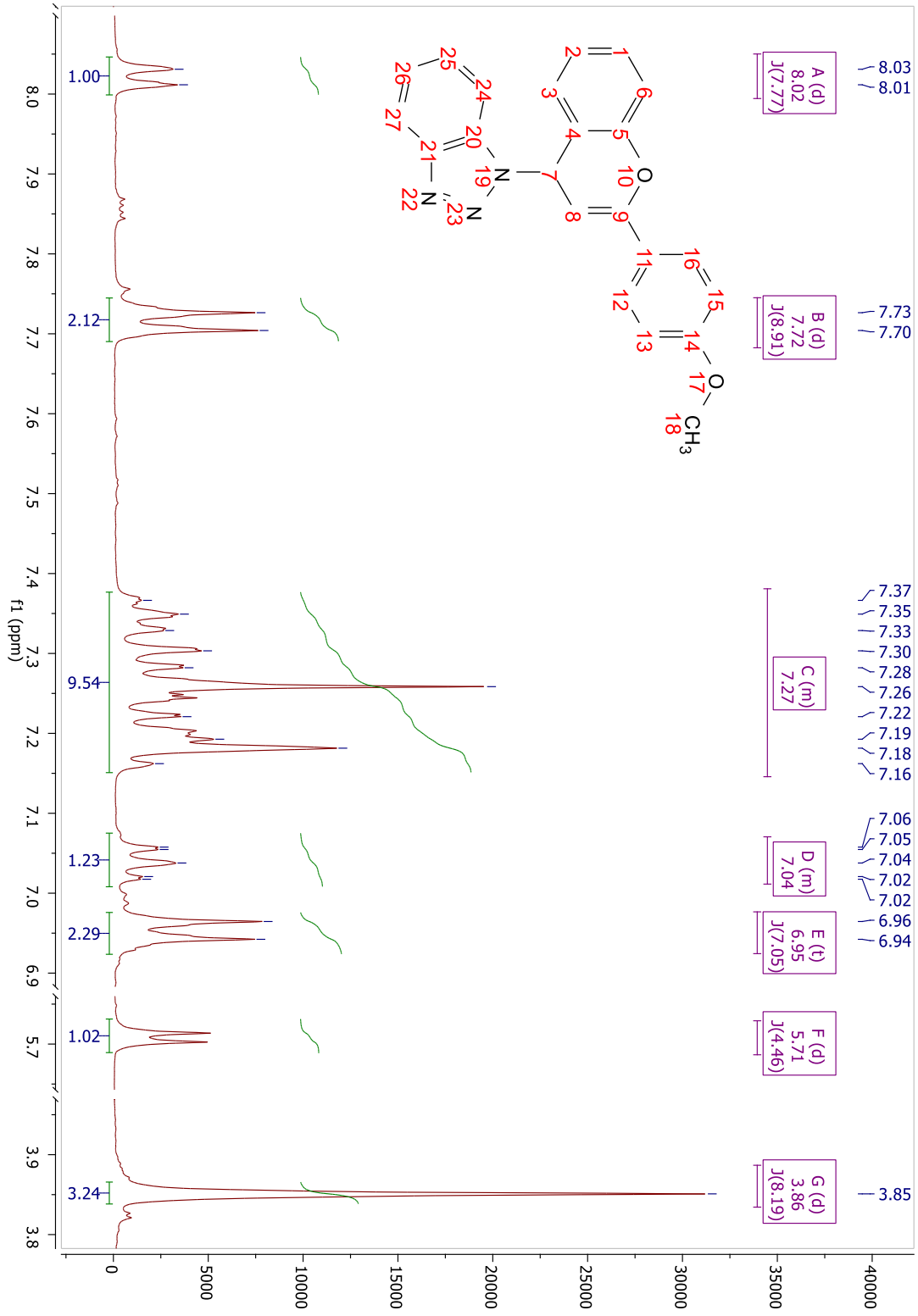

^{1}H NMR spectra of 4-(bromomethyl)acetophenone (4)

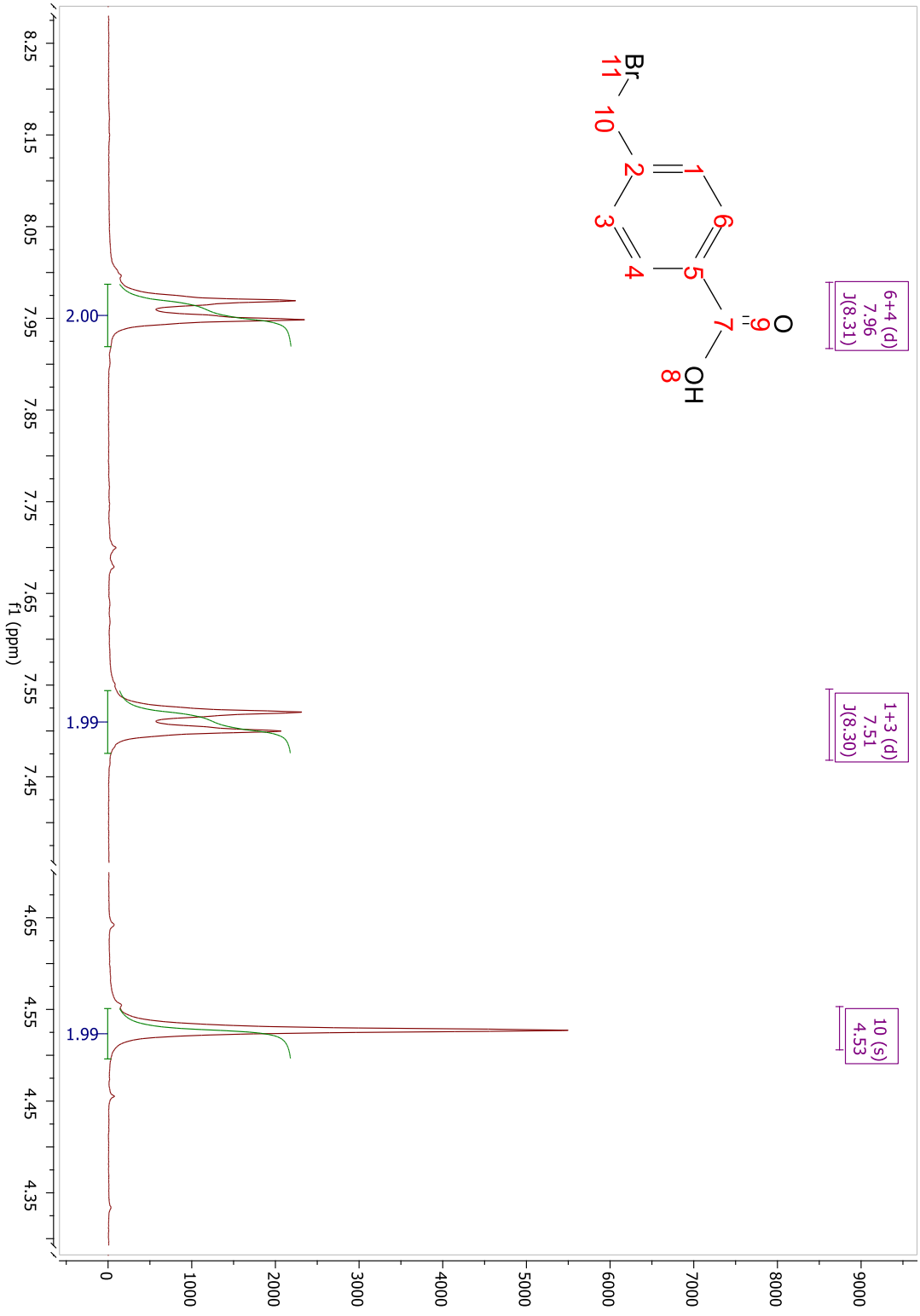

^{1}H NMR spectra of (4-Acetylphenyl)acetonitrile (5)

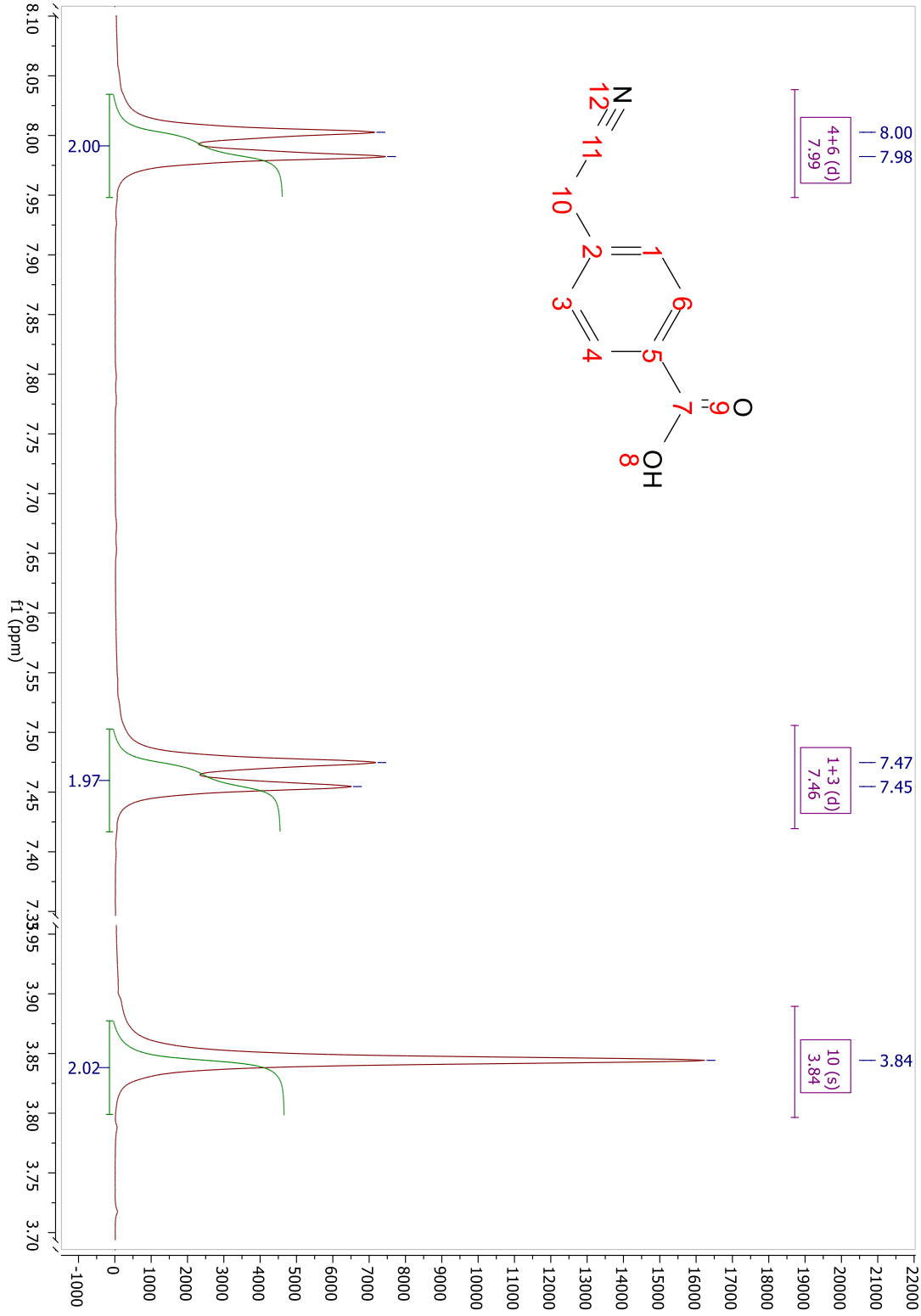

^{13}C NMR spectra of (4-Acetylphenyl)acetonitrile (5)

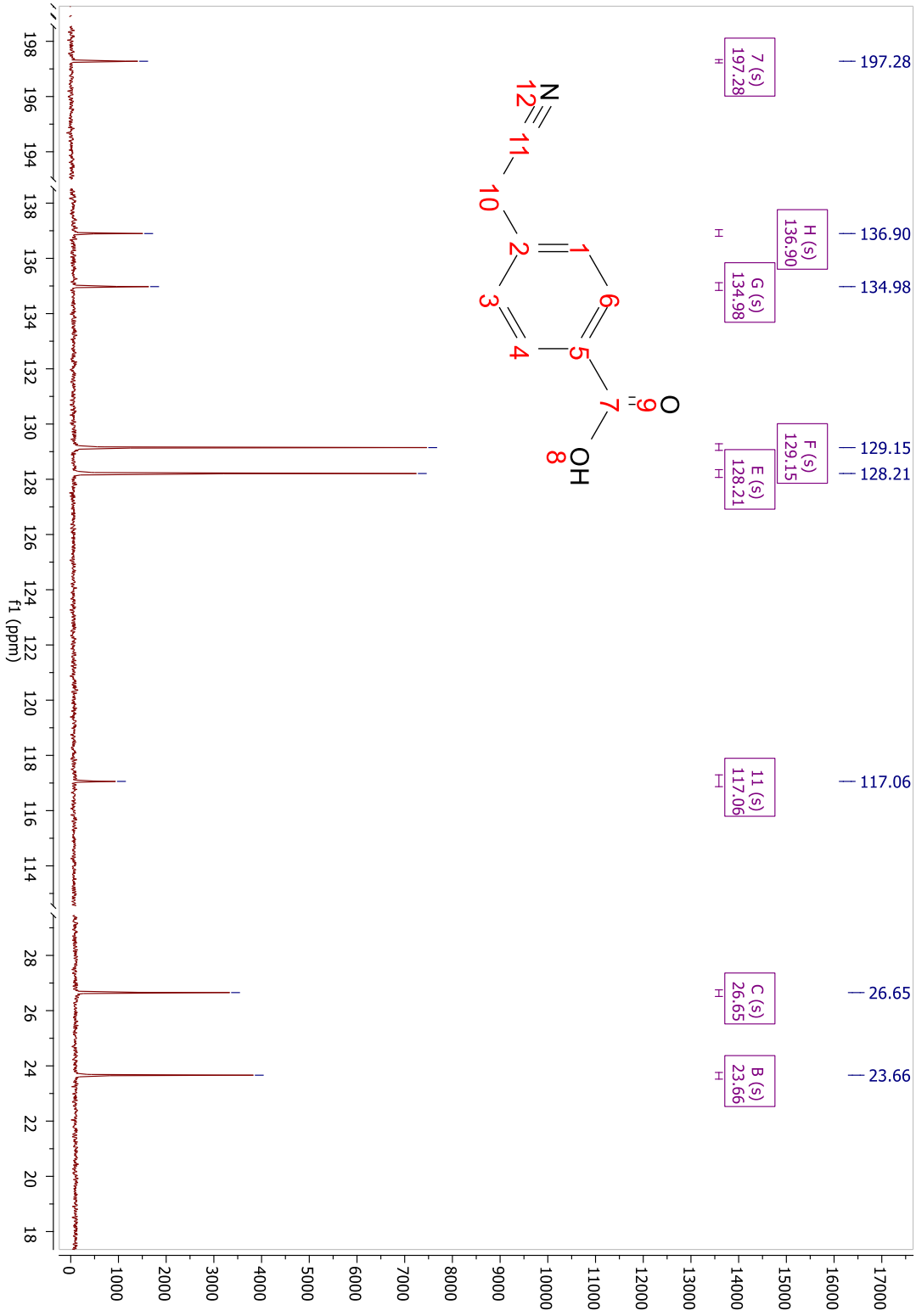

^{1}H NMR spectra of (4-Acetylphenyl)acetic acid (6)

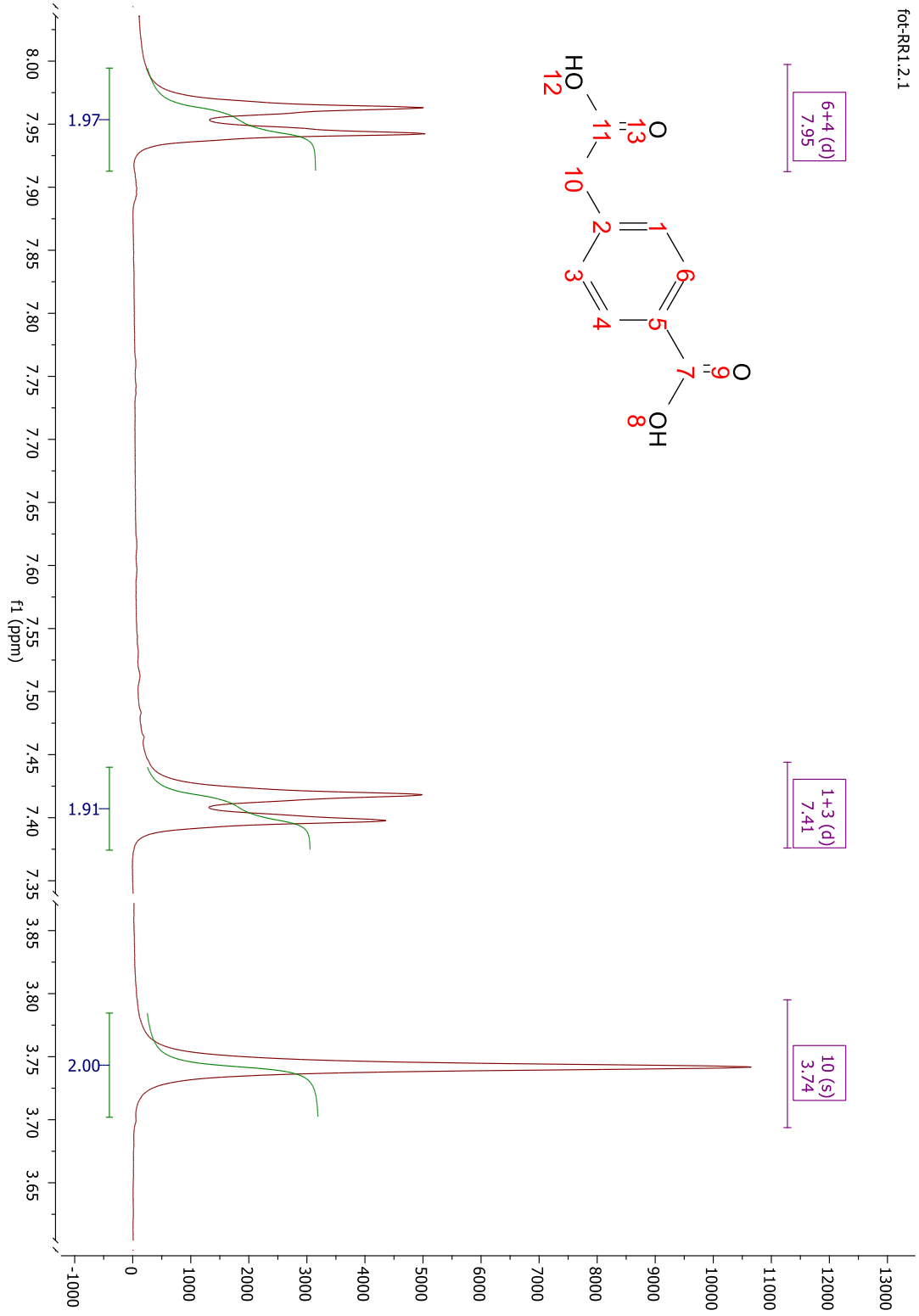

^{13}C NMR spectra of (4-Acetylphenyl)acetic acid (6)

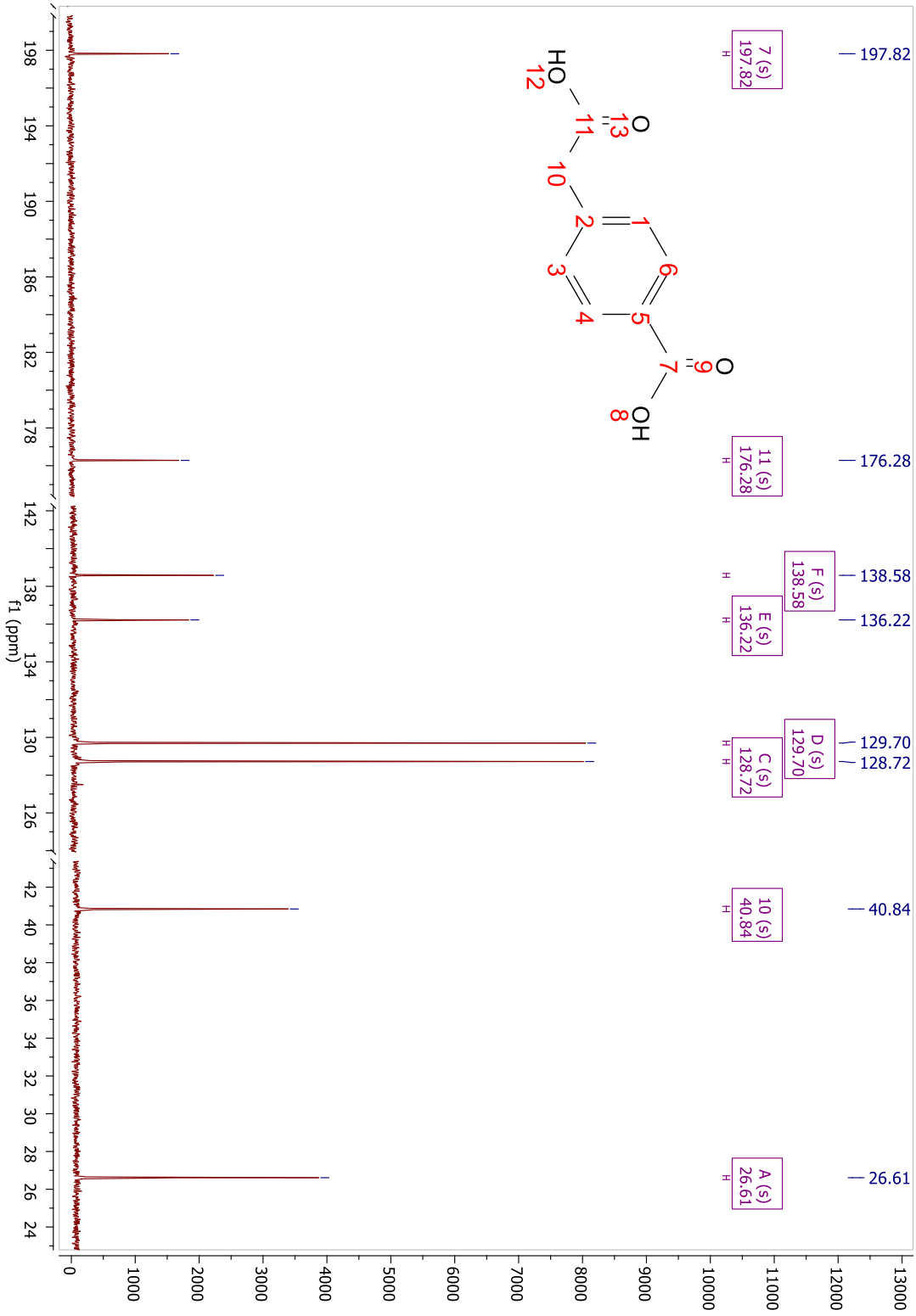

^{1}H NMR spectra of 4′-methylcarboxyflavylium (7)

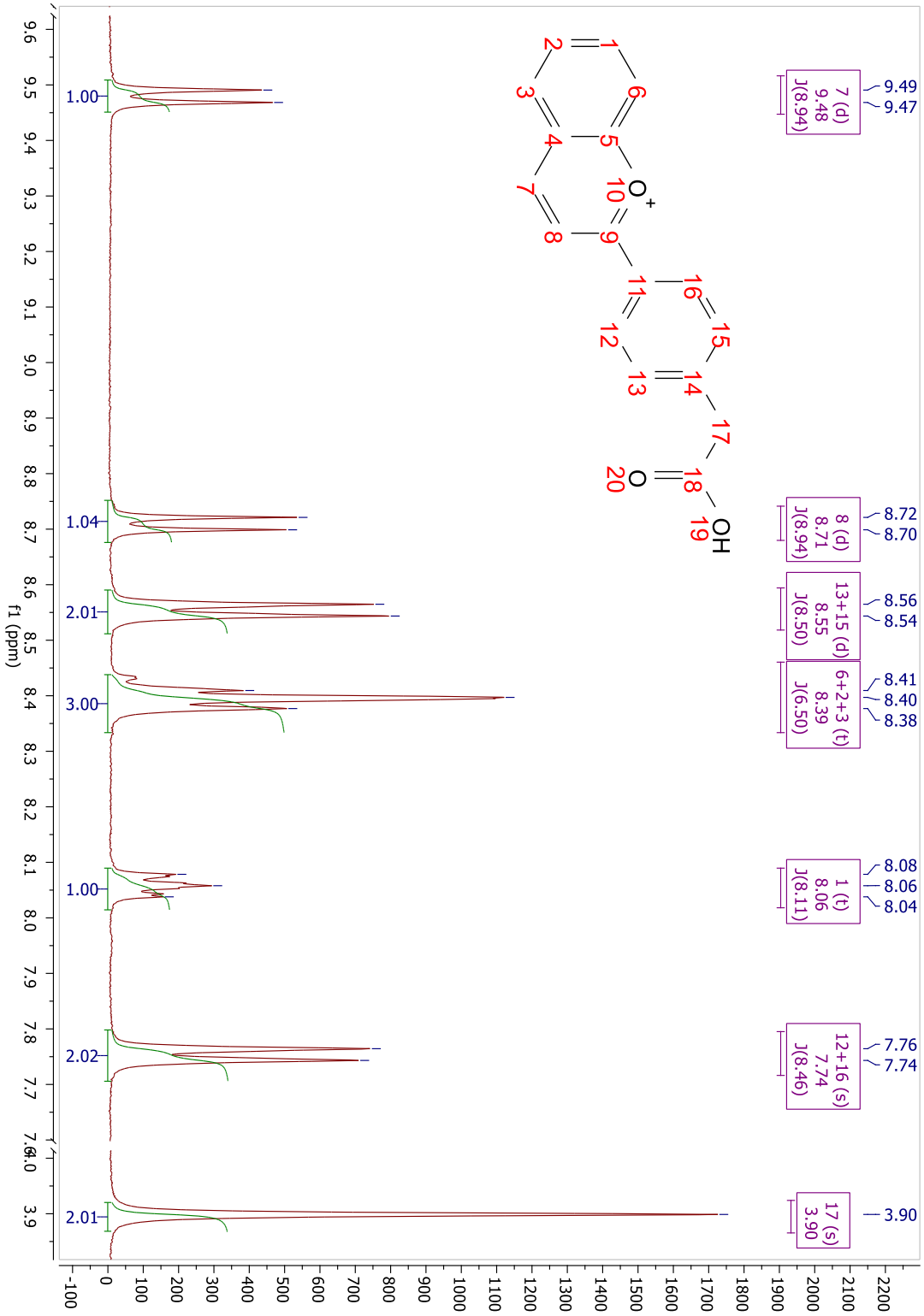

^{1}H NMR spectra of 7-hydroxy-4′-methylcarboxyflavylium (8)

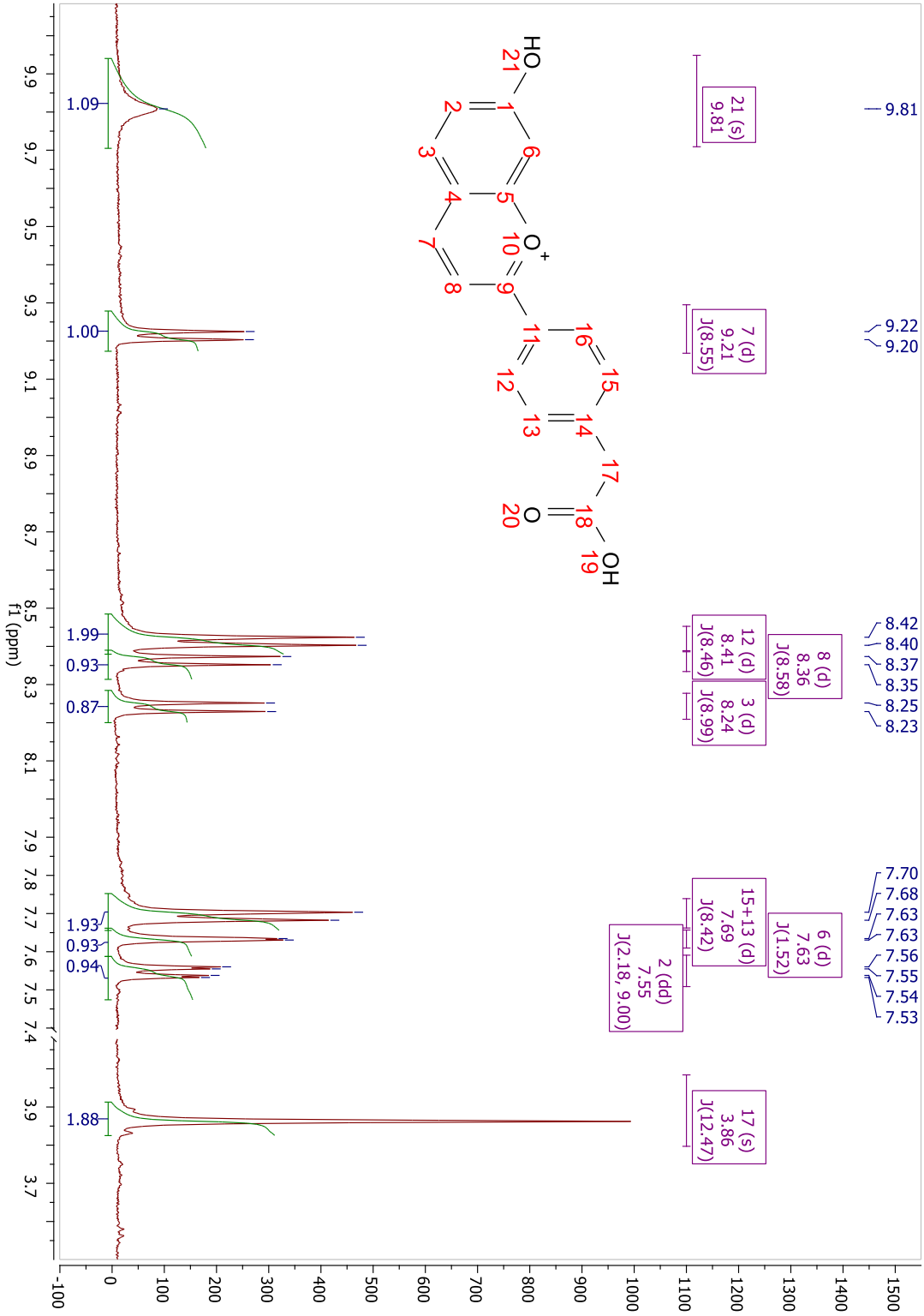

^{1}H NMR spectra of 4′-methylcarboxychalcone (9)

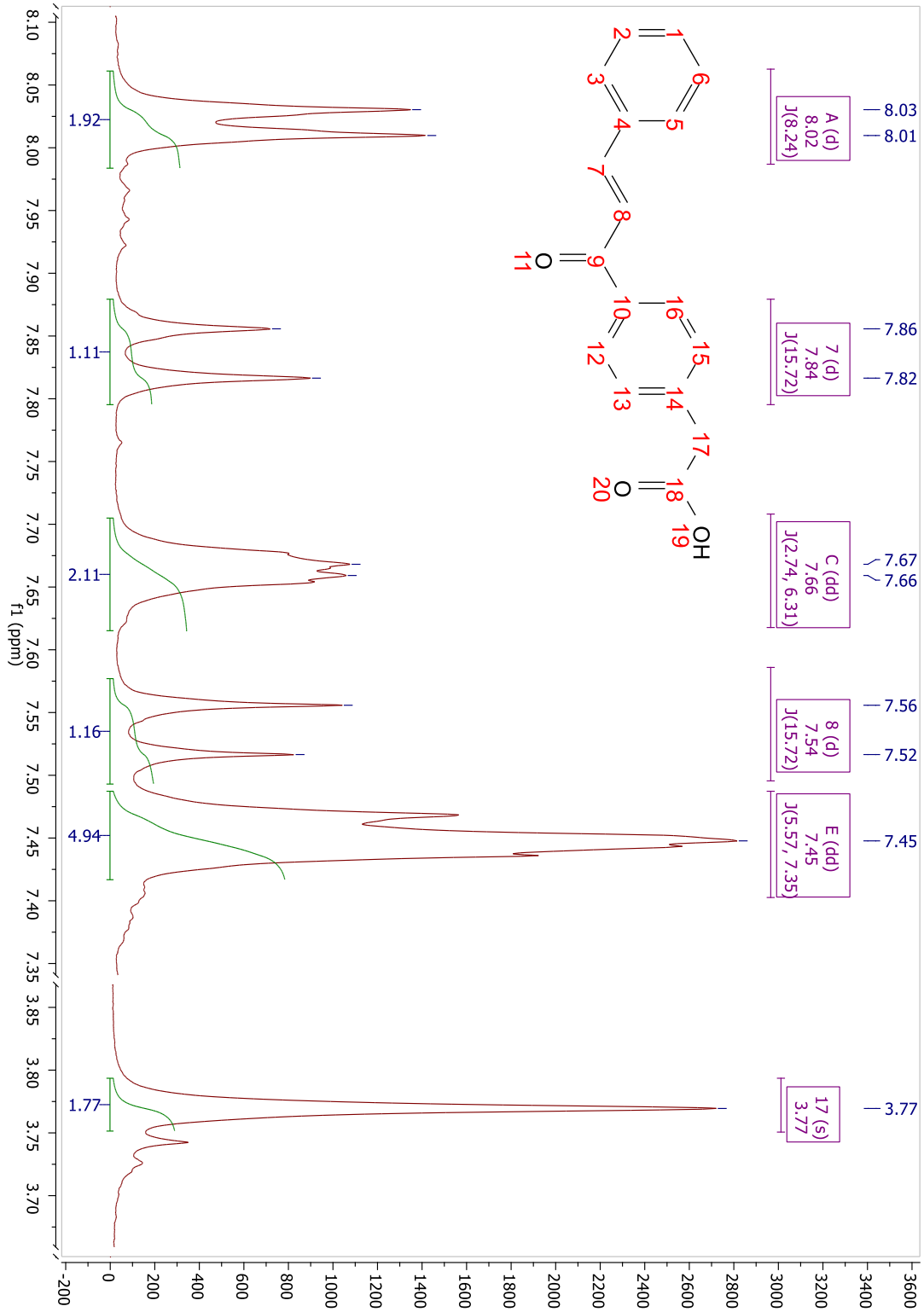

^{1}H NMR spectra of 7-hydroxy-4′-methylcarboxy-4-phenylflavylium (10)

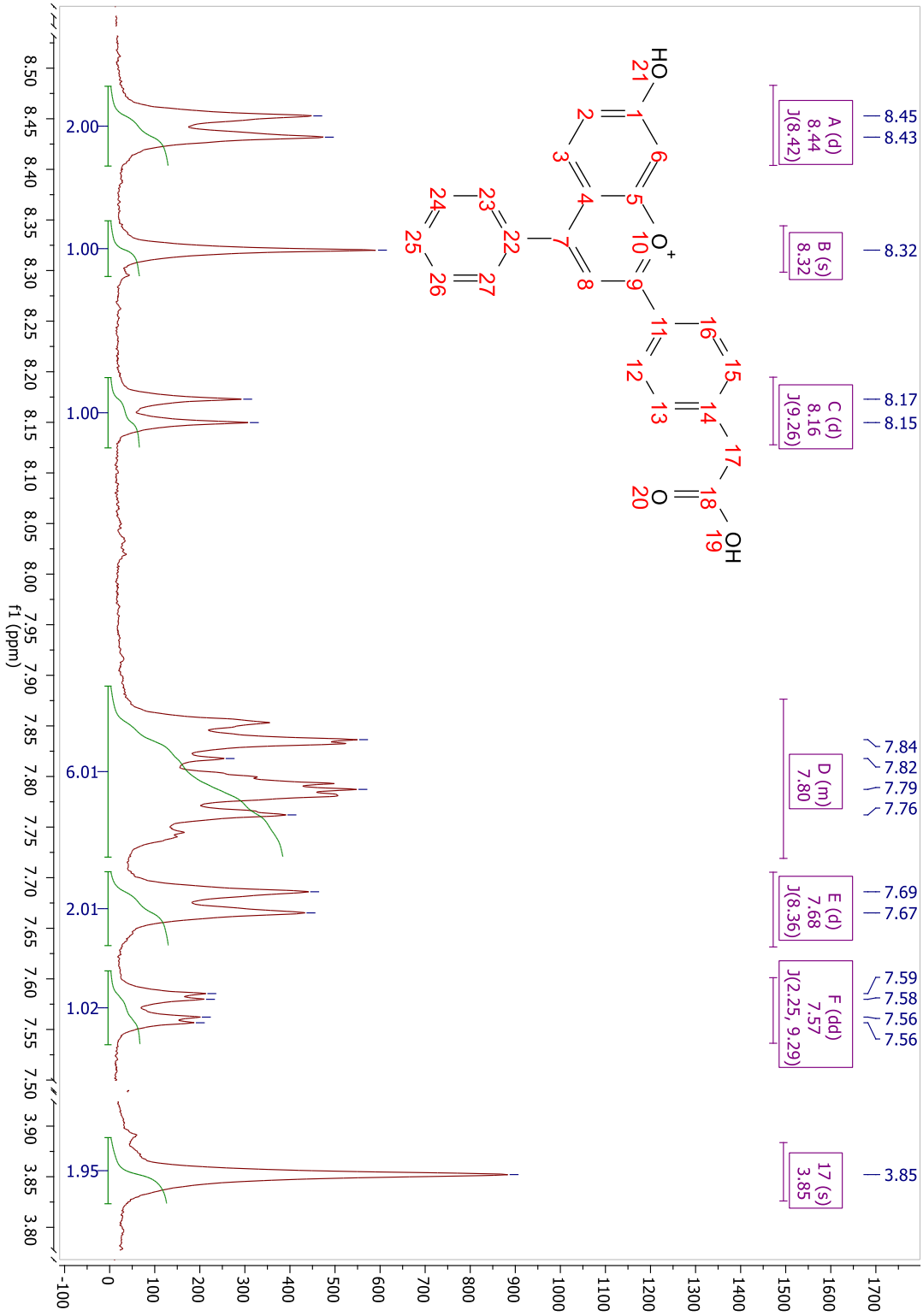

References

1 F. Jahnke, M. Kira and S. Koch, *Dwc.Knaw.Nl*, 2000, 101–110.

2 Y. Wang and A. Hu, *J. Mater. Chem. C*, 2014, **2**, 6921.

3 S. Y. Lim, W. Shen and Z. Gao, *Chem. Soc. Rev.*, 2014, **44**, 362–381.

4 A. P. Alivisatos, *Science (80-.).*, 1996, **271**, 933–937.

5 D. J. Norris and M. G. Bawendi, *Phys. Rev. B*, 1996, **53**, 16338–16346.

6 L. Liang and W. Xie, *Phys. B Condens. Matter*, 2015, **462**, 15–17.

7 K. J. Nordell, E. M. Boatman and G. C. Lisensky, *J. Chem. Educ.*, 2005, **82**, 1697.

8 M. L. Landry, T. E. Morrell, T. K. Karagounis, C. H. Hsia and C. Y. Wang, *J. Chem. Educ.*, 2014, **91**, 274–279.

9 W. K. Bae, J. Joo, L. A. Padilha, J. Won, D. C. Lee, Q. Lin, W. K. Koh, H. Luo, V. I. Klimov and J. M. Pietryga, *J. Am. Chem. Soc.*, 2012, **134**, 20160–20168.

10 X. L. Dai, Z. X. Zhang, Y. Z. Jin, Y. Niu, H. J. Cao, X. Y. Liang, L. W. Chen, J. P. Wang and X. G. Peng, *Nature*, 2014, **515**, 96–100.

11 Y. Q. Zhang, D. K. Ma, Y. G. Zhang, W. Chen and S. M. Huang, *Nano Energy*, 2013, **2**, 545–552.

12 U. Resch-Genger, M. Grabolle, S. Cavaliere-Jaricot, R. Nitschke and T. Nann, *Nat Meth*, 2008, **5**, 763–775.

13 S. Jin, Y. Hu, Z. Gu, L. Liu and H.-C. Wu, *J. Nanomater.*, 2011, **2011**, 1–13.

14 K. M. Tsoi, Q. Dai, B. A. Alman and W. C. W. Chan, *Acc. Chem. Res.*, 2013, **46**, 662–671.

15 X. Xu, R. Ray, Y. Gu, H. J. Ploehn, L. Gearheart, K. Raker and W. A. Scrivens, *J. Am. Chem. Soc.*, 2004, **126**, 12736–12737.

16 Y. P. Sun, B. Zhou, Y. Lin, W. Wang, K. A. S. Fernando, P. Pathak, M. J. Meziani, B. A. Harruff, X. Wang, H. Wang, P. G. Luo, H. Yang, M. E. Kose, B. Chen, L. M. Veca and S. Y. Xie, *J. Am. Chem. Soc.*, 2006, **128**, 7756–7757.

17 B. P. Biswal, D. B. Shinde, V. K. Pillai and R. Banerjee, *Nanoscale*, 2013, **5**, 10556–61.

18 S. Zhu, L. Wang, N. Zhou, X. Zhao, Y. Song, S. Maharjan, J. Zhang, L. Lu, H. Wang and B. Yang, *Chem. Commun. (Camb).*, 2014, **50**, 13845–8.

19 B. Zhang, C. Y. Liu and Y. Liu, *Eur. J. Inorg. Chem.*, 2010, 4411–4414.

20 W. Du, X. Xu, H. Hao, R. Liu, D. Zhang, F. Gao and Q. Lu, *Sci. China Chem.*, 2015, **58**, 863–870.

21 J. Briscoe, A. Marinovic, M. Sevilla, S. Dunn and M. Titirici, *Angew. Chemie - Int. Ed.*, 2015, **54**, 4463–4468.

22 V. Thongpool, P. Asanithi and P. Limsuwan, *Procedia Eng.*, 2012, **32**, 1054–1060.

23 J. Deng, Q. Lu, N. Mi, H. Li, M. Liu, M. Xu, L. Tan, Q. Xie, Y. Zhang and S. Yao, *Chem. – A Eur. J.*, 2014, **20**, 4993–4999.

24 P. Roy, P. C. Chen, A. P. Periasamy, Y. N. Chen and H. T. Chang, *Mater. Today*, 2015, **18**, 447–458.

25 Y. Guo, Z. Wang, H. Shao and X. Jiang, *Carbon N. Y.*, 2013, **52**, 583–589.

26 A. M. Vedran Milosavljevica Pavel Kopela, et al., *J. Met. Nanotechnologies*, 2014, 16–22.

27 X. M. Li, J. L. Chang, F. Xu, X. R. Wang, Y. H. Lang, Z. Y. Gao, D. P. Wu and K. Jiang, *Res. Chem. Intermed.*, 2015, **41**, 813–819.

28 S. Zhu, Y. Song, X. Zhao, J. Shao, J. Zhang and B. Yang, *Nano Res.*, 2015, **8**, 355–381.

29 B. Liao, P. Long, B. He, S. Yi, B. Ou, S. Shen and J. Chen, *J. Mater. Chem. C*, 2013, **1**, 3716–3721.

30 Z. Qian, X. Shan, L. Chai, J. Ma, J. Chen and H. Feng, *ACS Appl. Mater. Interfaces*, 2014, **6**, 6797–6805.

31 D. Qu, M. Zheng, L. Zhang, H. Zhao, Z. Xie, X. Jing, R. E. Haddad, H. Fan and Z. Sun, *Sci. Rep.*, 2014, **4**, 5294.

32 F. Pina, M. J. Melo, C. a. T. Laia, a. J. Parola and J. C. Lima, *Chem. Soc. Rev.*, 2012, **41**, 869.

33 F. Ito, N. Tanaka, A. Katsuki and T. Fujii, *J. Photochem. Photobiol. A Chem.*, 2004, **161**, 111–118.

34 F. Pina, M. Maestri and V. Balzani, *Chem. Commun.*, 1999, **35**, 107–114.

35 F. Ito, N. Tanaka, A. Katsuki and T. Fujii, *J. Photochem. Photobiol. A Chem.*, 2002, **150**, 153–157.

36 G. Chen, S. Wu, L. Hui, Y. Zhao, J. Ye, Z. Tan, W. Zeng, Z. Tao, L. Yang and Y. Zhu, *Sci. Rep.*, 2016, **6**, 19028.

37 A. R. Katritzky, P. Czerney, J. R. Levell and W. H. Du, *European J. Org. Chem.*, 1998, 2623–2629.

38 R. Robinson and J. Walker, *J. Chem. Soc.*, 1934, 1435–1440.